Continuous-Wave and Passively Mode-Locked Alexandrite Lasers Pumped at 532 nm

by

Shirin Ghanbari

A Thesis submitted to the Faculty of Graduate Studies of

The University of Manitoba

in partial fulfilment of the requirements of the degree of

Doctor of Philosophy

Department of Electrical and Computer Engineering

University of Manitoba

Winnipeg

In the Name of God

"The knowledge of anything, since all things have causes, is not acquired or complete unless it is known by its causes."

(Abu Ali Sina)

To

my mother Azam,

my father Amir Hossein and

my sister Maryam.

Abstract

Alexandrite crystal (Cr-ion doped chrysoberyl, Cr^{3+}: $BeAl_2O_4$) is an attractive gain medium for producing ultrashort laser pulses. Alexandrite properties are similar to those of the Ti:sapphire crystal, which is the most widely used crystal for creating ultrashort pulses. Therefore, Alexandrite can be a good candidate for development of ultra-short pulse lasers. To date, the generation of femtosecond pulses from an Alexandrite laser has not been reported. The primary aim of this research was to create an ultrashort pulse Alexandrite laser. In the first stage of this research, a continuous- wave Alexandrite laser was designed, built and optimized to provide maximum output power. Also, its laser beam quality and wavelength tuning range using a single plate birefringent filter was measured. In addition, the basic behavior of the laser to determine its thermal lensing was investigated. Furthermore, a dual-wavelength operation using several single plate birefringent filters was demonstrated for the first time. In the second stage of this research, ultrashort pulses of 420 fs and 380 fs duration from a quantum-dot saturable absorber mode-locked Alexandrite laser were obtained for the first time. Finally, a femtosecond Kerr-lens mode-locked Alexandrite laser that produced 170 fs long pulses was created for the first time. These results can lead to the development of efficient ultrafast Alexandrite oscillators and amplifiers that can replace widely used inefficient and costly Ti:sapphire laser systems.

Acknowledgements

First, I would like to thank God for giving me strength to achieve my goals.

These achievements could not have been possible without the love, constant support, help and encouragement that my mother Azam, my father Amir Hossein and my sister Maryam have given me during this difficult journey.

I would like to express my gratitude to my advisor Professor Arkady Major whose research has been inspirational. Furthermore, I would like to thank him for helping me use my capabilities to accomplish this significant achievement.

I am also thankful for my committee members, Professor Behzad Kordi, Professor Jitendra Paliwal and Professor Dan Popescu, who took their time to give me valuable comments.

I want to thank Dr. Haitao Zhao for his advice and my other colleagues for creating a friendly and joyful environment in which to work.

Finally, I gratefully acknowledge the financial and academic support from the University of Manitoba and the financial support from the Natural Sciences and Engineering Research Council of Canada (NSERC) and the Canada Foundation for Innovation (CFI).

Table of Contents

List of Tables

List of Figures

List of Symbols and Abbreviations

Symbols

M^2	Beam quality parameter (M-squared)
θ_B	Brewster's angle
r	Distance from the center of a beam
σ	Emission cross-section
n_e	Extra ordinary refractive index
τ	Fluorescence lifetime
ν	Frequency
f	Focal length
w_c	Laser mode radius
λ_c	Laser wavelength
I	Light intensity
Z	Light propagation direction
ΔR	Modulation depth
n_2	Nonlinear refractive index
ΔR_{ns}	Nonsaturable loss
η_{opt}	Optical-to-optical efficiency
λ_0	Peak lasing wavelength
h	Planck constant
w_p	Pump radius
λ_p	Pump wavelength

n	Refractive index
F_s	Saturation fluence of the gain medium
$F_{sat,A}$	Saturation fluence of the SESAM
η	Slope efficiency
η_{abs}	Slope efficiency with respect to the absorbed pump power
c	The speed of light
d	Thickness of birefringent filter
λ	Wavelength

Abbreviations

BRF	Birefringent filter
Cr	Chromium
CW	Continuous-wave
FWHM	Full width at half maximum
HR	Highly reflecting
KLM	Kerr-lens mode locking
ML	Mode locking
OC	Output coupler
QD-SESAM	Quantum-dot semiconductor saturable absorber mirror
RF	Radio frequency
$sech^2$	Hyperbolic secant function squared
SESAM	Semiconductor saturable absorber mirror

Chapter 1: Introduction

1.1 Research Rationale, Objectives, and Scope

Laser (Light Amplification by Stimulated Emission of Radiation) means that a highly coherent light can be obtained by stimulated emission [1]. Laser-active media with broadband gain are widely employed for the generation of ultrashort pulses [2–5] (as short as a few 10^{-15} seconds, i.e. femtoseconds). In fact, ultrafast laser sources in the near-infrared spectral region are highly desirable for a wide range of applications, including ultrafast spectroscopy [6-8], nonlinear frequency conversion [9-11], nonlinear microscopy [12-15], and optical coherence tomography for imaging biological tissues with micro-scale resolution [16-18]. In addition, the extremely short pulses (down to the level of several femtoseconds) permit one to observe the ultrafast dynamics of ions and molecular rearrangements [19]. Also, the high peak intensity of such lasers can lead to the absorption of two or multiple photons, which is employed in nonlinear imaging methods with subcellular 3-D resolution and deep penetration depth [20, 21]. Moreover, with intense femtosecond pulses, materials are destroyed inside the restricted region of focus so fast that the heat has no time to diffuse out of the focal volume, resulting in an accurate and clean cut. In fact, high pulse energy laser sources are favored in the micromachining field. At the same time low pulse energy sources are appropriate in nanosurgery for delicate biological matters. Such ultrashort pulses of light are typically produced by laser gain media which have broad emission bandwidths [22, 23]. Currently, Ti:sapphire is the most commonly used broadband vibronic laser crystal that can directly generate a few cycle optical pulses [24, 25]. On the other hand, Alexandrite (Cr-doped chrysoberyl $BeAl_2O_4$) is another example of vibronic laser crystal [26] that has a wide (~100 nm) wavelength tuning range around 750 nm and high thermal conductivity (similar to Ti:sapphire) [27,

28]. Its other advantages are highly polarized output radiation and broad absorption bands that can be used for a direct pumping with visible laser diodes [29, 30]. Unlike Ti:sapphire, Alexandrite can be directly pumped with red laser diodes because its absorption band covers most of the visible spectral range [26, 29]. In addition, its larger $\sigma\tau$ product [31] presents a prospect of lower laser threshold. Furthermore, a diode-pumped Alexandrite laser was shown to produce >26 W of output power in the continuous-wave regime [29] which significantly exceeds output from widely used Ti:sapphire lasers.

Ti:sapphire is a golden standard to produce ultra short pulses. According to the Table 1.1, when compared to a widely used Ti:sapphire crystal, Alexandrite has a longer fluorescence lifetime τ (262 μs at room temperature) and a lower stimulated emission cross section σ (0.7×10^{-20} cm^2). On the other hand, the higher $\sigma\tau$ product of Alexandrite indicates the possibility of an efficient laser action with low threshold. In addition, as illustrated in Figure 1, absorption bands of Alexandrite extend into the red part of the visible spectrum (600-680 nm regions) where laser diodes are available; however, the absorption of Ti:sapphire does not cover the red part of the spectrum, peaking at 490 nm in the blue-green region. Indeed, red diode pumped Alexandrite lasers can provide higher quantum efficiency when compared with the blue and green pump wavelengths [29-33]. Furthermore, the index of refraction is almost the same for both Ti:sapphire and Alexandrite crystals.

Table 1.1. Material parameters of Alexandrite and Ti:sapphire [1, 27, 32].

Parameters	Alexandrite	Ti:sapphire
Laser wavelength (nm)	700-820	670-1070
Maximum gain wavelength (nm)	755	790
Emission cross section σ (cm^2)	0.7×10^{-20} (E‖b-axis)	4.1×10^{-19} (E‖c-axis)
		2.0×10^{-19} (E ⊥ c-axis)
Fluorescence lifetime τ (μs)	262	3.2
Index of refraction (@ 750 nm)	1.74	1.76

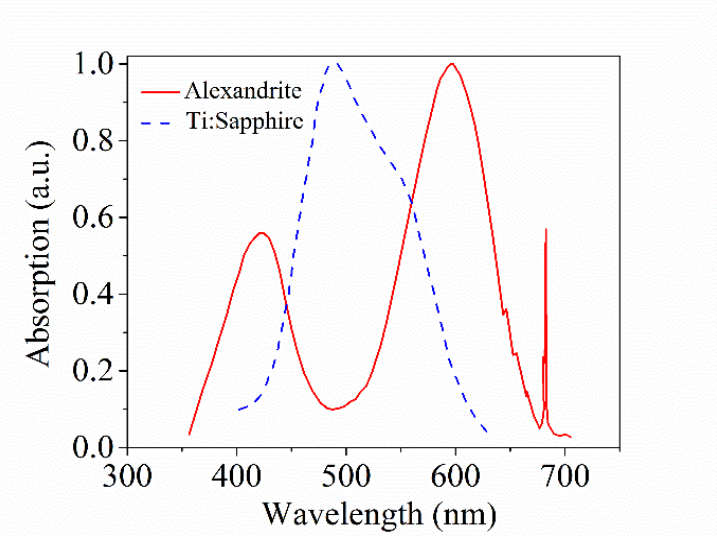

Figure 1.1. Normalized absorption spectra of Alexandrite (solid line, E‖b-axis) [34] and Ti:sapphire (dashed line, E‖c-axis) [1].

Thus, Alexandrite can be a good candidate to replace Ti:sapphire. In fact, Alexandrite has the potential to be mode-locked effectively because of its broad gain bandwidth and energy storage abilities to provide high peak power pulses. Therefore, a mode-locked Alexandrite laser can have an efficient, simple, and reliable structure if diode pumping is implemented.

Properties of the Alexandrite crystal that make it suitable for creating ultrashort pulses are its broad range of wavelength tunability, its wide absorption spectra which include green and red wavelength ranges, its thermo-mechanical strength, and its low threshold pump power. Despite all of these attractive features, mode locking performance of Alexandrite was demonstrated only in the picosecond regime, producing 8 ps pulses as the shortest [35]. The main objective of this work was the generation of ultrashort pulses from Alexandrite laser through a mode locking technique.

1.2 Thesis Organization, Contributions, and Novelty

This thesis is comprised of four journal papers and organized in six chapters as follows:

Chapter 1: Introduction

An introduction to the thesis is given in this chapter that summarizes the research objectives and scope. In addition, this chapter provides a comparison between widely used femtosecond laser source, Ti:sapphire, and Alexandrite that motivates the investigation of the latter.

Chapter 2: Properties of the Alexandrite crystal

The optical and physical performance and properties of the Alexandrite crystal are described in this chapter.

Chapter 3: High power continuous-wave Alexandrite laser with green pump.

[28] S. Ghanbari and A. Major, "High power continuous-wave Alexandrite laser with green pump," *Laser Physics*, vol. 26, no. 7, p. 075001, 2016.

- Thermo-optical properties of Alexandrite laser crystal (submitted)

In this chapter, after introduction and literature review, the experimental setup for a high power continuous-wave (CW) laser oscillator was discussed. Then, the fundamentals of thermal lensing effect are reviewed and the thermal lensing properties of the Alexandrite laser are discussed. The contributions and novelty of this chapter are:

- A high power continuous-wave Alexandrite laser with a maximum output power of 2.6 W at 755 nm was demonstrated using a Brewster-angled crystal pumped with up to 11 W of 532 nm laser. A slope efficiency of 26% was obtained. Also, a broad tuning range of 85 nm and a fundamental laser mode operation were demonstrated. These results were necessary to gain my other publications of short pulses.
- The focal length of the thermal lens was experimentally determined and reported for the first time for the 532 nm pumped Alexandrite laser.

Chapter 4: High power continuous-wave dual-wavelength Alexandrite laser

S. Ghanbari and A. Major, "High power continuous-wave dual-wavelength alexandrite laser," *Laser Physics Letters*, vol. 14, no. 10, p. 105001, 2017.

This chapter reports on the development of a high power continuous-wave tunable dual-wavelength Alexandrite laser system using a single plate birefringent filter. In this section, after

an introduction, the theoretical background of generating dual-wavelength laser by using a single plate birefringent filter is discussed. Then, the experimental setup is described and the results are explained. The contribution and novelty of this chapter is:

- Demonstration of a high power continuous-wave tunable dual-wavelength Alexandrite laser for the first time. Using a 6 mm thick BRF, dual-wavelength output at 745.2 nm and 756.2 nm with 850 mW of average output power was obtained with 16.8% of optical-to-optical and 24.2% of slope efficiency. Also, the dual-wavelengths with similar output powers were obtained using the 4 mm and 2 mm thick BRFs.

Chapter 5: Femtosecond Alexandrite laser passively mode-locked by an InP/InGaP quantum-dot saturable absorber

S. Ghanbari, K. Fedorova, A. Krysa, E. Rafailov and A. Major, "Femtosecond Alexandrite laser passively mode-locked by an InP/InGaP quantum-dot saturable absorber," *Optics Letters*, vol. 43, no. 2, p. 232, 2018.

In this chapter, the development of a femtosecond quantum-dot SESAM mode-locked Alexandrite laser is discussed. After an introduction, the experimental setup and results are presented. Contributions and novelty of this chapter is:

- First report on stable mode-locked operation of an Alexandrite laser based on a quantum dot saturable absorber. Stable femtosecond pulses with 380 and 480 fs duration at ~775 nm and an average output power of 295 and 325 mW were generated from a green radiation pumped Alexandrite laser passively mode-locked by an InP/InGaP quantum-dot semiconductor saturable absorber mirror.

Chapter 6: Femtosecond Kerr-lens mode-locked Alexandrite laser

[51] S. Ghanbari, R. Akbari and A. Major, "Femtosecond Kerr-lens mode-locked Alexandrite laser,"*Optics Express*, vol. 24, no. 13, p. 14836, 2016.

This chapter reports on the Kerr-lens mode-locked Alexandrite laser. After describing the Kerr-lens mode locking concept, the experiment is discussed and results are presented. Then, future improvements are explained. The contributions and novelty of this chapter are:

- This chapter describes the demonstration of pure Kerr-lens mode locking of an Alexandrite laser for the first time. The femtosecond pulses of 170 fs pulse duration at 755 nm were obtained with 780 mW of output power. The laser was pumped at 532 nm and the optical-to-optical efficiency of 9.8% was achieved.
- This was the shortest pulse duration produced from Alexandrite laser at the time of this work.

Chapter 7: Conclusions and Future Work

This chapter summarizes the presented material, and outlines the future work of this research.

Chapter 2: Properties of the Alexandrite Crystal

Alexandrite (Cr^{3+}: $BeAl_2O_4$), a rare gemstone composed of Cr (transition metal) in the host crystal, has its optical transitions occur between the coupled vibrational and electronic states. Therefore, the emission of a photon is associated with the emission of a phonon which makes it a vibronic laser. The Alexandrite laser has a high thermo-mechanical strength which makes it an attractive laser gain medium for high power/energy operations as well as the generation of ultrashort pulses. It has high thermal conductivity and a broad emission wavelength span ranging from 700 to 820 nm. Its laser performance is increased at elevated temperatures due to the increase of its stimulated emission cross section [27]. Alexandrite has broad absorption bands extending from ~320 to 690 nm with peaks at ~425 and 600 nm (see Figure 1) [34]. In addition, there is a narrow strong absorption peak at ~680 nm. The crystal is birefringent (biaxial orthorhombic) and therefore provides a highly-polarized laser emission which eliminates depolarization loss [27]. The gain in Alexandrite for the polarization along the crystal b-axis, E||b, is about 10 times higher than the gain for the polarization along the crystal a-axis, E||a, and the polarization along the crystal c-axis, E||c. Higher pump absorption can also be achieved for the E||b polarization [34].

2.1 Physical Properties of the Alexandrite Crystal

Alexandrite (Cr^{3+}: $BeAl_2O_4$) consists of four units of $BeAl_2O_4$ providing an orthorhombic structure [36]. The crystal has high thermo-mechanical and chemical stability, high thermal conductivity, and high strength which make it a suitable host for high power lasers. An important parameter of a laser gain medium is doping density. Doping density, which can enhance the pump absorption coefficient, can be as high as 0.3% in Alexandrite crystal. Its optimum Cr^{3+} concentration is determined by its rod length, pump source, and applications. This crystal has the

ability to maintain high gain and efficiency at higher temperatures when compared with other solid-state lasers. In Table 2.1 the physical properties of Alexandrite are shown.

Table 2.1. Thermal and mechanical properties of Alexandrite crystal [27, 32].

Thermal expansion, ‖b-axis (K^{-1})	6×10^{-6}
Thermal conductivity (W/m/K)	23
Melting point (°C)	1870
Hardness (kg/mm^2)	2000
Breaking stress (GPa)	0.457 - 0.948
Young's modulus (GPa)	469
Thermo-optic coefficient, ‖b-axis (K^{-1})	8×10^{-6}

2.2 Optical Properties of the Alexandrite Crystal

Alexandrite is an orthorhombic crystal. It means that Alexandrite has three crystallographic axes (*a, b, c*) [36] which have different polarized absorption and emission cross sections as explained in the next section. Figure 2.1 shows c-axis view of Alexandrite structure [37].

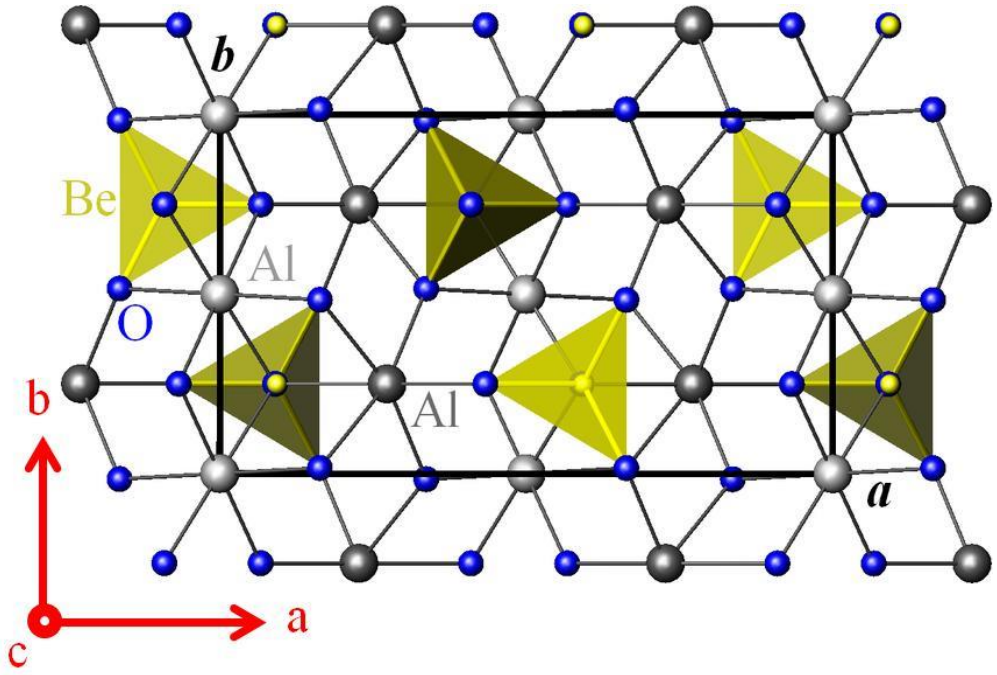

Figure 2.1. c-axis view of Alexandrite structure [37].

2.2.1 Emission and Absorption Spectra of the Alexandrite Crystal

Alexandrite crystal contains trivalent chromium ions which cause its broad absorption and emission bands [1]. Alexandrite crystal has broad absorption bands of around 380 to 630 nm with peaks at 410 and 590 nm. Moreover, there is a narrow absorption peak at 680 nm. Alexandrite lases with flash-lamp pumps at a room temperature in the 700 - 820 nm range.

Because of the crystal structure, the light absorption in the 500-680 nm range with the E||b polarization is higher than the absorption for the E||a and E||c polarizations (Figure 2.2) [1, 34]. Also, polarized emission is another advantage of Alexandrite for lasing performance as it controls thermal birefringence and prevents depolarization loss during laser operation [27].

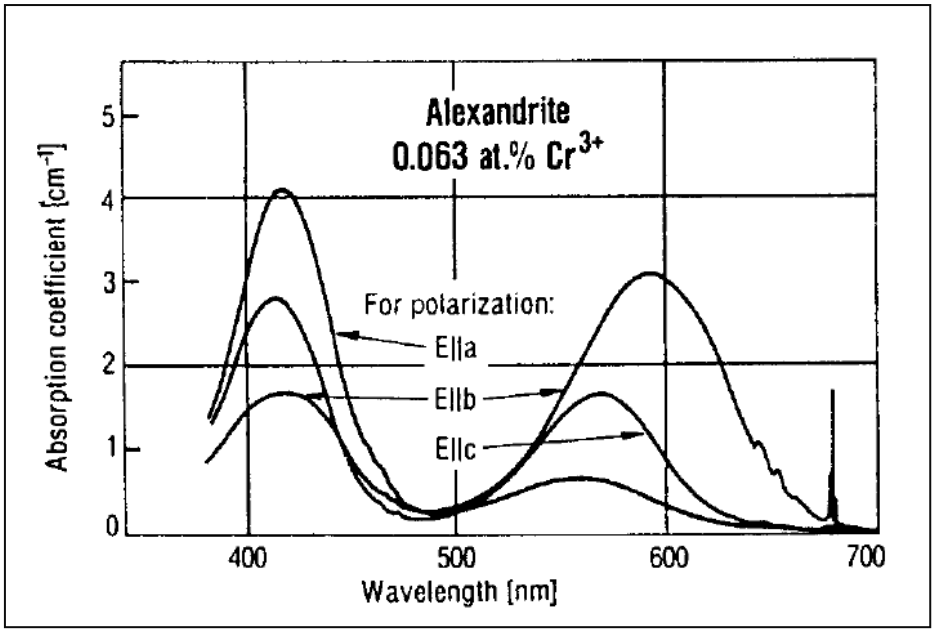

Figure 2.2. Absorption spectra of the Alexandrite crystal for different crystal axis. Used with the permission of Springer Nature [1].

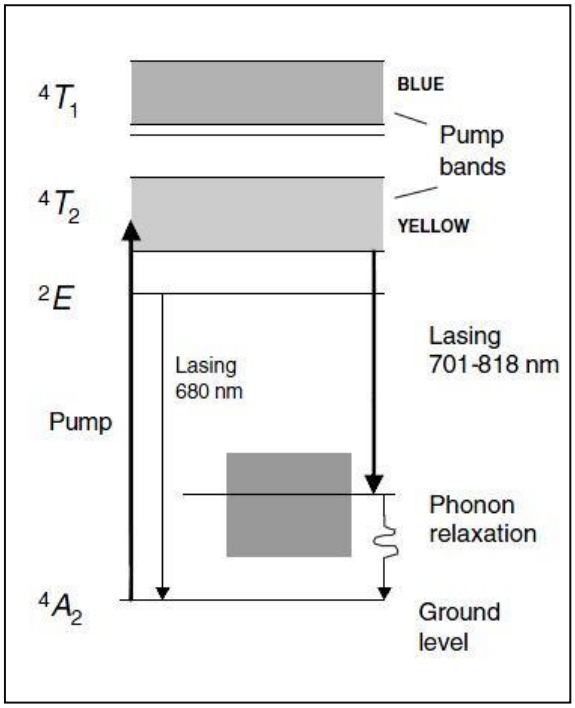

Figure 2.3. Energy levels of the Alexandrite crystal. Used with the permission of Springer Nature [1].

Gain cross section of Alexandrite increases at a higher temperature, so the laser performance is improved by heating the laser rod. Alexandrite crystal can operate as a four-level vibronic laser system (main interest) or a three-level basic laser system (R-line at 680 nm similar to Ruby). The energy states of Alexandrite crystal are illustrated in Figure 2.3.

In the three-level system, transitions occur from the storage level (^2E) to the ground level ($^4A_2$). This three-level system has a high threshold, fixed output wavelength (680.4 nm at room temperature), and relatively low efficiency. However, in a four-level system, transitions from $^4T_2$ to $^4A_2$ energy levels provide the main emission spectra. In fact, Alexandrite lasing occurs due to electronic $^4T_2$-$^4A_2$+$\hbar w_{phonon}$ transitions which provide a wide range of frequencies (700-820 nm) at room temperature. The absorption spectra include two broadband transitions from $^4A_2$ to $^4T_1$ energy states in the 510-690 nm wavelength range and from $^4A_2$ to $^4T_2$ energy states in the 380-480 nm wavelength range both of which are in the visible range. The $^4T_2$ energy states have a 260 µsec lifetime. In fact, due to the vibronic nature of the Alexandrite crystal, the emission of a photon is followed by the emission of phonons, so it provides a broad tunability of around 120 nm which will be explained in the next chapter [1, 38]. Thus, this laser crystal is suitable for producing broadly tunable CW operation and ultrashort pulses because of its broad emission band which is due to electronic vibrational transition.

Furthermore, the ^2E energy state of Alexandrite crystal acts as a storage state for $^4T_2$ when thermal excitation causes ^2E populations to transfer to $^4T_2$. In this way, ^2E supplies $^4T_2$ with electrons at elevated temperatures. Also, according to the Boltzmann distribution, since the energy difference between ^2E and $^4T_2$ states is 800 cm^{-1}, the population in $^4T_2$ is always much smaller than the population in the ^2E state, so the transferring of populations from ^2E to $^4T_2$ energy levels in the Alexandrite crystal is beneficial for the Alexandrite laser performance. Therefore, the gain of

Alexandrite rises when the temperature is increased, since the ^2E state supplies electrons to $^4T_2$. Indeed, its emission cross section of about 0.5×10^{-20} cm^2 at room temperature (300K) increases by 10 times at 475 K. However, increasing temperature causes the maximum gain to move to a longer wavelength. In fact, increasing the temperature also provides more population in the lower lasing level of the Alexandrite crystal However, laser performance in general will be improved with larger electron populations at a high lasing level and smaller populations at a terminal lasing level. Therefore, increasing the temperature of the crystal has two opposite consequences. First, a higher temperature causes the upper laser level population to increase which is good for the laser performance. The second consequence of increasing the temperature is that the growth of the ground population has a negative impact on the laser performance. In fact, as a laser system heats up, the higher population of electrons at the terminal lasing level causes the laser to operate at longer wavelengths. As a result, only at wavelengths above 730 nm, the laser performance can be improved by increasing the temperature. Also, for maximum laser emission energy storage, there is an optimum temperature because the gain rises with the temperature, but the fluorescent lifetime decreases. On the whole, increasing the temperature of the Alexandrite crystal beyond an optimum point leads to lasing at longer wavelengths which consequently causes a decrease in its output power [39, 40, 41].

2.2.2 Performance of the Alexandrite as a Laser Gain Medium

As Alexandrite crystal is a high energy storage material, it is capable of generating high intracavity fluence. However, high fluence can cause an optical damage of the Alexandrite crystal rod, which becomes a limiting factor. Also, due to its low emission cross-section and high saturation fluence (in the 7-25 J/cm^2 range, depending on temperature), high laser fluence (the optical energy delivered per unit area) is needed to extract stored energy during laser operation.

Therefore, the high laser fluence used in low emission cross-section gain media can lead to optical damage. Saturation fluence (F_s) for a four level laser system is defined by equation (2.1) [1] where h is the Planck constant, ν is the frequency and σ is the stimulated emission cross section.

$$F_s = \frac{h}{\nu\sigma} \tag{2.1}$$

Additionally, since rod operational temperature is significant in optimizing general efficiency, high temperature helps to increase gain and energy extraction, but it results in increased fluorescence loss [27].

In conclusion, the Alexandrite crystal has a broad emission spectrum that makes it suitable for producing ultra short pulses. Also, the Alexandrite crystal is a high energy storage material, making it a desirable option for use in high power laser applications. The next chapter presents a high-power continuous-wave Alexandrite laser with a green pump which is the fundamental step in mode locking of the Alexandrite laser and the main goal of this thesis.

Chapter 3: High Power Continuous-Wave Alexandrite Laser with Green Pump

In continuous-wave (CW) or free running mode all frequency components of the laser oscillate without fixed amplitude and phase relationships which causes constant time-averaged laser output power. In this section, the operation of a CW Alexandrite ($Cr:BeAl_2O_4$) laser, pumped by a high power green source at 532 nm with a diffraction limited beam is reported. An output power of 2.6 W at 755 nm, a slope efficiency of 26%, and wavelength tunability of 85 nm have been achieved using 11 W of green pump. To the best of our knowledge, this is the highest CW output power of a high brightness laser pumped Alexandrite laser reported to date. In this chapter, the principles of CW laser are described. Then, after a brief review of the previous results in a CW regime, the experimental setup and the results of CW Alexandrite laser in this work are presented.

3.1 Existing Continuous-Wave Alexandrite Laser Pumping Methods

Alexandrite can be pumped with different methods such as flash lamp, laser diode, and green lasers. To provide a comparison with earlier laser reports, Table 3.1 presents a summary of different pumping methods used with CW Alexandrite lasers. For example, when pumped with 6 kW arc flash lamp (Xenon) Alexandrite laser produced output power of 60 W with 1% slope efficiency [27]. The highest output power for CW operation of a diode-pumped (at 639 nm) Alexandrite lasers reached 26.2 W using 64.5 W of pump power, with slope efficiency of 49% and a wavelength tunability of 62 nm [29]. Also, a laser diode at 680.4 nm with pump power of 865 mW and another one at 678.5 nm with pump power of 925 mW were used as the pump sources for Alexandrite to achieve 200 mW of output power with 34% slope efficiency and 168 mW of output

with 38% slope efficiency, respectively [31]. Moreover, a diode laser at 635 nm with 170 mW of power was used as a pump source to produce 48 mW of output power with 36% slope efficiency and 68 nm of wavelength tuning [42]. In another experiment, a 1.9 W Krypton ion laser at 647.1 nm was used as a pump for Alexandrite to produce 600 mW of output power with 51% slope efficiency and 76 nm of wavelength tuning range [43]. Unfortunately, this pumping method cannot provide high output power due to its limited pump power. In addition, a dye laser at 645 nm pumped Alexandrite with ~0.36 W of pump power and produced 0.15 W of output power with the highest to date slope efficiency of 64% [33]. Nevertheless, pumping with dye lasers is not practical due to their complexity and low efficiency. An alternative approach to improving output power is to use high power diffraction limited green pump sources at 532 nm that are widely used with Ti:sapphire lasers. In fact, the Alexandrite laser with 1.4 W of output power and wavelength tunability of 50 nm has already been demonstrated [44]. Among all of these pumping methods the green pump has the highest brightness, can achieve output powers of >20 W and is commercially available.

In this thesis, a 532 nm pump was used to successfully produce a high power Alexandrite laser with 2.6 W of output power. In addition, wavelength tuning over 85 nm was achieved using a single plate birefringent filter (BRF). To the best of our knowledge, this is the highest CW output power and the broadest wavelength tunability of a high brightness laser-pumped Alexandrite laser reported to date. The demonstrated Alexandrite laser is very attractive for the development of ultrafast mode-locked Alexandrite lasers and high-power tunable solid-state UV laser sources using frequency conversion.

Table 3.1. Performance of Alexandrite lasers.

Pump Source	Pump power	Output power	Slope efficiency	Tuning range	References
Arc flash lamp (He)	6 kW	60 W	1%	-----	[27]
Red laser diode (639 nm)	64.5 W	26.2 W	49%	62 nm	[29]
Red laser diode (680.4 nm)	0.865W	0.2 W	34%	-----	[31]
Red laser diode (678.5nm)	0.925 W	0.168 W	38%	86 nm	[31]
Red laser diode (635nm)	0.17 W	0.048 W	36%	68 nm	[42]
Ion laser (Krypton at 647.1 nm)	~1.9 W	0.6 W	51%	76 nm	[43]
Dye laser (645 nm)	~0.36 W	0.15 W	64%	-----	[33]
Green laser (532 nm)	5 W	1.4 W	31%	50 nm	[44]
Green laser (532 nm)	11 W	2.6 W	26%	85 nm	This work
Green laser (532 nm)	5 W	1.24 W	29%	-----	This work

3.2 Experimental Setup

Experimental setup of a CW Alexandrite oscillator is schematically depicted in Figure 3.1 and consisted of four mirrors and a Brewster-angled crystal. The designed cavity provided a good overlap between the pump and cavity modes. M1 is a highly reflecting (HR) at 650-900 nm. The radii of curvature of the two HR concave mirrors M2 and M3 were 10 cm. A 3 mm × 7 mm Alexandrite crystal slab (Solix Ltd.) doped with 0.3% of Cr^{3+} was used in the experiments. The crystal was held in an aluminum crystal holder and was not actively cooled. It was mounted on

a translation stage which helped to optimize its position with respect to the pump and cavity mode foci. The crystal was pumped with up to 11 W of CW green laser radiation at 532 nm (Finesse, Laser Quantum). The pump had a low divergence TEM_{00} spatial mode and was focused into a ~44 μm spot size diameter inside the Alexandrite crystal by a 150 mm focal length lens. About 95% of the pump power was absorbed inside the crystal. In the experiments the used output coupler mirrors had four different transmissions of 0.75%, 3%, 5% and 8% around 755 nm.

(a)

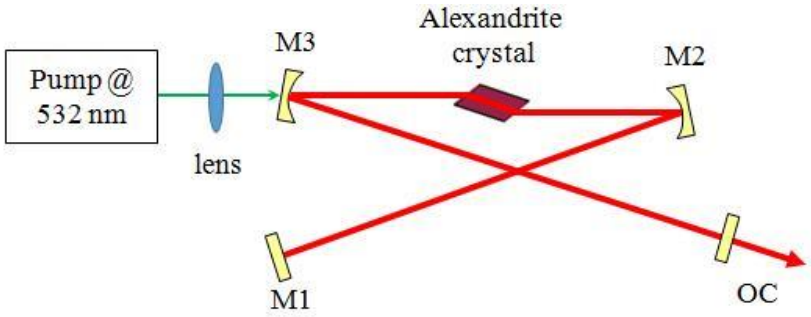

(b)

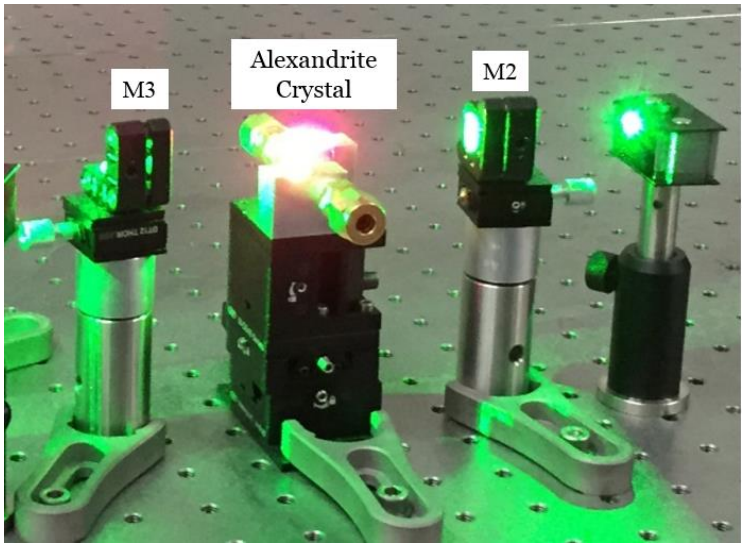

Figure 3.1. (a) Schematic of the CW Alexandrite laser. M1 is an HR flat mirror. M2-M3 are the HR concave mirrors. OC is the output coupler. (b) A photo of the pumped Alexandrite crystal placed between M2 and M3.

3.3 Results and Discussion

During the experiments a spontaneous fluorescence spectrum of Alexandrite crystal was measured by blocking one of the cavity arms. The result is demonstrated in Figure 3.2 which shows the fluorescence that spans from ~650 nm to 800 nm. A single peak on the left side belongs to the pump laser at 532 nm. In a three-level Alexandrite laser system, it emits at ~680 nm as shown in the Figures 2.3 and 3.2.

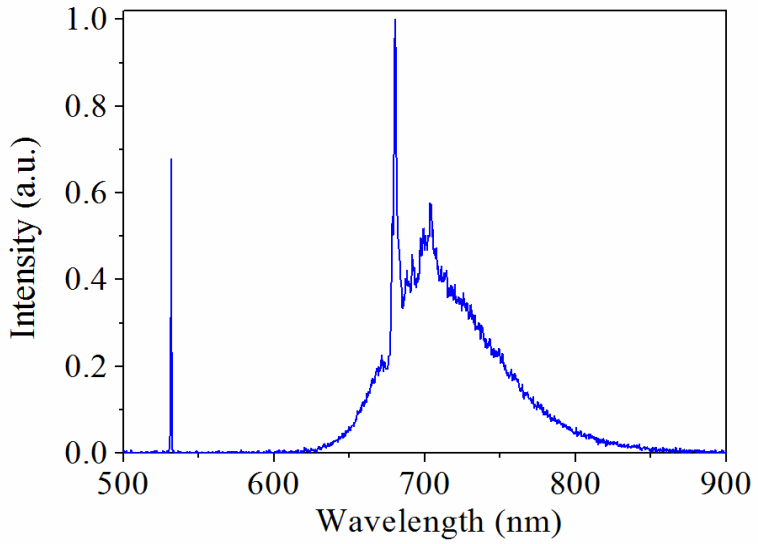

Figure 3.2. Spontaneous fluorescence spectra of Alexandrite crystal excited at 532 nm.

The measured CW output power versus the pump power for different output couplers is shown in Figure 3.3. A maximum output power of 2.6 W was achieved in free running mode with 755 nm central wavelength using 5% output coupler. This corresponds to a slope efficiency of 26% and an optical-to-optical efficiency of 24%. They are a bit lower than Kuper and Brown's previously reported 31% and 32%, respectively [44], shown as a dashed line in Figure 3.3. This lower slope and optical-to-optical efficiency can be explained by a higher level of intracavity loss

due to the possible slight misalignment of the used crystal from the perfect condition of the Brewster angle of incidence. Furthermore, this intracavity loss can be due to the increased number of mirrors in the cavity. Kuper and Brown used only one mirror in a semi-monolithic cavity, which accounts for their higher efficiency. However, the laser developed in this study has higher output power and ability to implement mode locking.

The laser spectrum at the maximum output power in free running mode is illustrated in Figure 3.4. The spectrum spans ~30 nm from 740 nm to 770 nm.

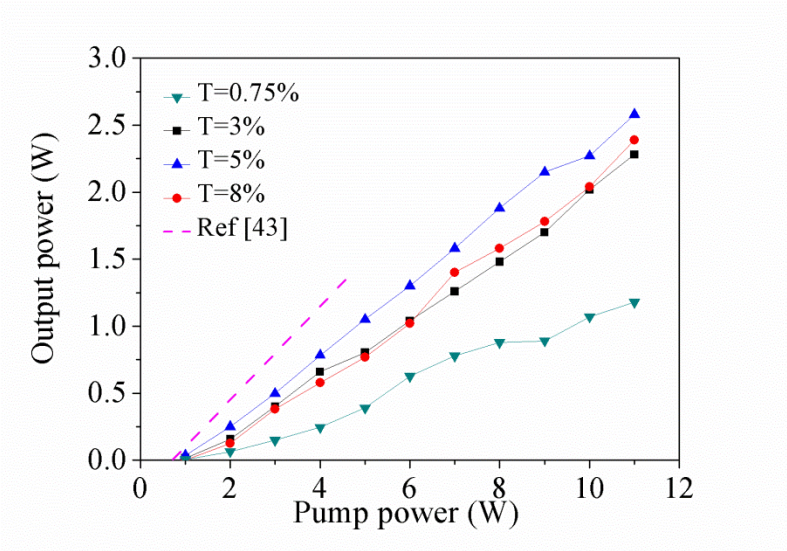

Figure 3.3. Continuous-wave output power of Alexandrite laser versus pump power using 0.75%, 3%, 5%, and 8% output couplers.

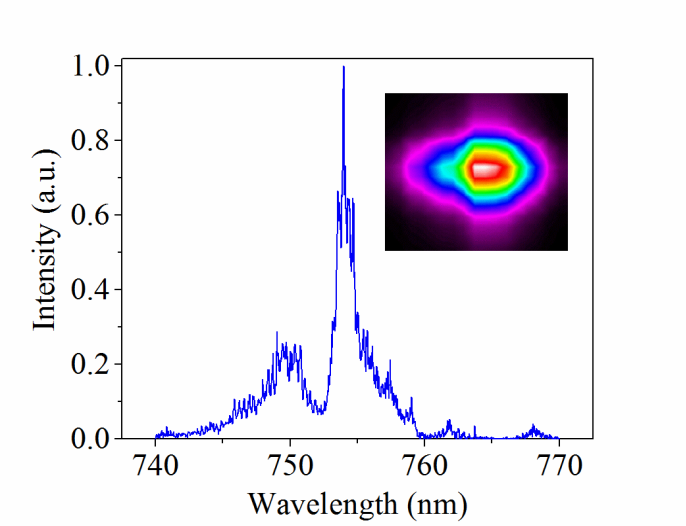

Figure 3.4. Laser spectrum in free running mode for 5% OC and laser beam shape at 2.6 W of output power.

The transverse beam intensity profile for 2.6 W of output power was measured by a CCD camera and is also shown in Figure 3.4 as an inset. The non-circular shape with the beam quality factors of $M^2_X = 5.99$ and $M^2_Y = 2.32$ is the evidence of thermal lensing effects in the laser crystal.

A single transverse mode beam with a circular shape and beam quality factors of $M^2_X = 1.5$ and $M^2_Y = 1.2$ could also be achieved with 1.24 W of output power (see figure 3.5) by adjusting the length of both cavity arms to provide a better mode matching with the pump. In this case, a slope efficiency of 29% and an optical-to-optical efficiency of 25% was obtained.

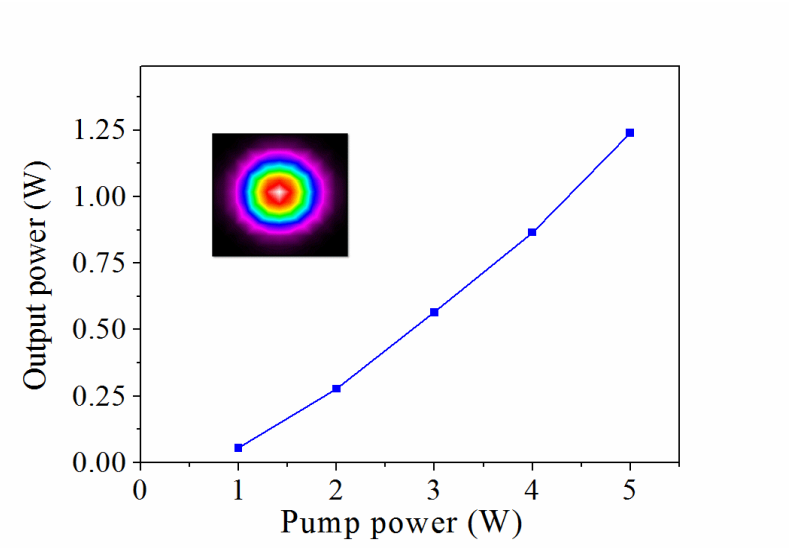

Figure 3.5. Output power versus pump power in improved beam quality regime. Inset: laser beam profile at full power.

In this experiment, tunability of the laser wavelength was also explored using a single birefringent plate (BRF) tuner with 0.5 mm thickness. It was placed in one of the resonator arms at Brewster's angle to minimize insertion losses. The laser could be continuously tuned from 715 nm to 800 nm. The measured output power versus wavelength is demonstrated in Figure 3.6.

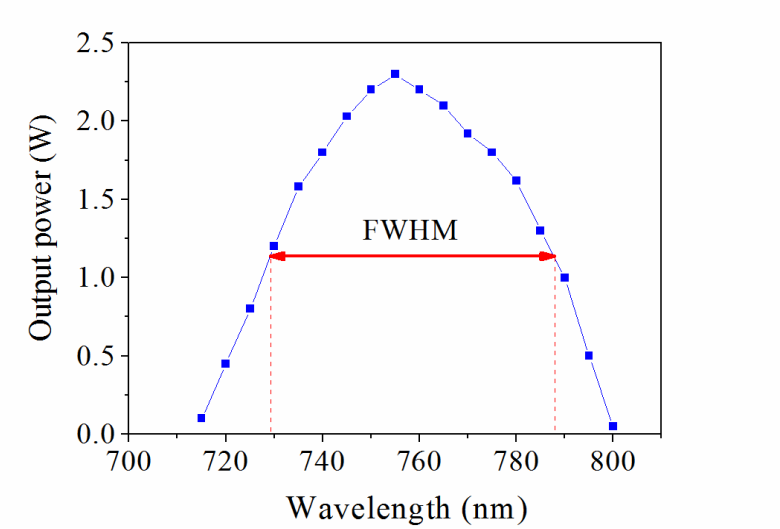

Figure 3.6. Alexandrite output power versus wavelength using 0.5 mm BRF. FWHM = 58 nm. The output coupler had 95% reflectivity across this spectral range.

As can be seen, the maximum output power was reached at 755 nm and the full width at half maximum (FWHM) of the wavelength tuning range was 58 nm. The laser line narrowed spectrum for the maximum output power is displayed in Figure 3. 7.

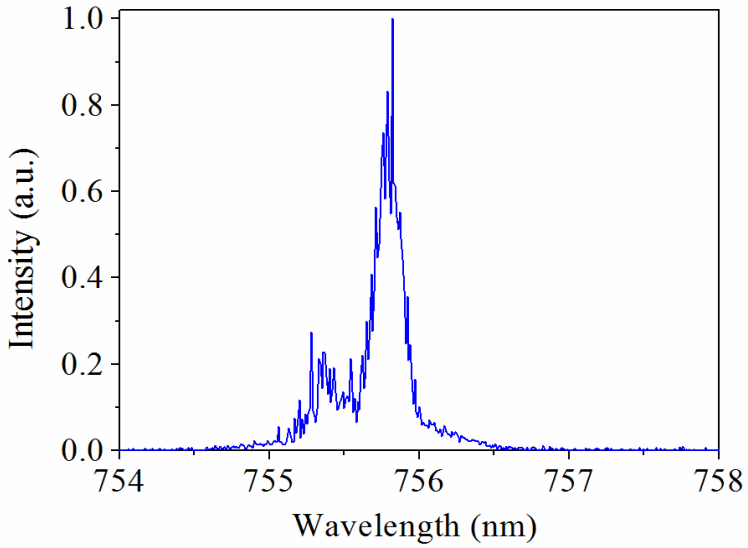

Figure 3.7. Laser spectrum at the maximum power using 0.5 mm BRF.

Similar spectral features such as in Figure 3.7 could be achieved in all of the observed 85 nm tunability range from 715 nm to 800 nm. The observed smooth wavelength tunability and tuning range suggest that Alexandrite is a promising gain medium for ultrashort pulse generation down to ~10 fs.

This chapter described a high-power broadly tunable operation of an Alexandrite laser pumped at 532 nm. The laser produced up to 2.6 W of output power in a free running CW regime. This is the highest output power achieved to date in a high brightness laser-pumped configuration. A slope efficiency of 26% has been achieved with a slightly multimode output. The output wavelength was tunable from 715 to 800 nm with a FWHM of 58 nm. A single transverse mode output with 1.24 W and slope efficiency of 29% has also been achieved.

3.4 Thermal Lensing in Continuous-Wave Alexandrite Laser

Thermal lens determination in a solid-state laser is one of the most important factors in laser design and performance. High pump power causes considerable heat generation in a laser crystal which leads to a thermal lensing effect. When a lasing medium is excited by high optical pumping, the thermal gradient ΔT induces a spatial refractive index gradient Δn which creates the thermal lens. In fact, as the temperature rises, thermal lensing can be caused by the three reasons: refractive index variation due to temperature, mechanically-induced end face deformation and stress induced refractive index variation. Thermal lensing disturbs the stability and performance of a resonator. In addition, it limits the output power and compromises the beam quality of solid state lasers. Alexandrite is capable of tolerating a high pump power without damage owing to its good mechanical and thermal strength. Regardless of these facts, no in depth studies of thermal effects in Alexandrite lasers have been described to date. The estimation of thermal lensing is needed to

ensure the appropriate performance of high power laser oscillators. Thermal lensing can be minimized with proper pumping and cooling of a laser rod.

Alexandrite tolerates a high pump power without breakage, owing to its high mechanical strength. Regardless, thermal lensing correction is still needed in the Alexandrite laser so that an appropriate cavity can be designed in order for the high power laser oscillators to perform appropriately. In fact, heating of the crystal decreases fluorescence lifetime and shifts the operating wavelength of Alexandrite laser from ~760 nm to a longer one at ~803 nm [42]. As a laser crystal heats up, more electrons populate the higher state laser levels, but high populations also occur in lower laser levels and especially the higher terminal level will be filled with more electrons which produce longer wavelengths [1] In this CW experiment [28] such a wavelength shift was not observed indicating that the temperature rise in the crystal was not significant. Therefore, because the emission cross section increases at elevated temperatures [39] as it was explained in Chapter 1, the crystal was not actively cooled. There are two reasons that long wavelengths provide higher thermal lensing. The first reason is that the gain cross section is lower at longer wavelengths, so more pump power is needed to compensate for the lower gain cross section. The second reason is that the increased excited state emission and absorption at longer wavelengths generates more heat which leads to more thermal lensing [1, 39].

Another problem that occurs due to thermal lensing is depolarization. However, Alexandrite's intrinsic birefringence caused by its orthorhombic structure can compensate for the depolarization caused by thermal stress. This natural birefringence operation [26] is beneficial to the laser performance since it controls any depolarization induced by thermal lensing.

Different methods were developed for measuring of thermal lensing by others. These techniques include passing a probe beam, interferometric techniques, studying the cavity instability region, characterizing the beam with a wave front sensor, beam width measurement and ABCD modeling [1]. In this work, beam width measurement and ABCD modeling are used for determining the focal length of the thermal lens. The following sections report on the measurement of the focal length of the induced thermal lens for a Brewster-angled Alexandrite crystal which produced 1.11 W of output power in free-running mode. The crystal was end pumped with a 6 W of continuous-wave green pump radiation at 532 nm. Following this measurement, a focal lens of 114 mm horizontally and 83 mm vertically was determined at 6W of incident pump power.

3.4.1 The Thermal Lensing of the Alexandrite Laser

There are various reasons that cause heat generation in solid-state lasers. The main reason is the quantum defect, which is the difference between the pump energy photon and the emitted laser photon energy. This is shown in the following equation [1]:

$$q = (1 - \frac{\lambda_p}{\lambda_c}) \times 100\% . \qquad (3.1)$$

In equation (3.1), λ_p is the pump wavelength and λ_c is the laser light wavelength.

As indicated in Table 2.1, finite thermal conductivity of the Alexandrite creates a temperature gradient inside the crystal. This leads to a thermo-optic effect, which changes the refractive index inside the crystal. Also, the temperature gradient inside the crystal causes thermally induced mechanical stress. Through a photo-elastic effect, this mechanical stress causes more variations in the refractive index. Moreover, at high temperatures thermal expansion results in the bulging of the end faces of the crystal, which could damage the crystal. The induced refractive

index and bulging provide a lensing effect known as thermal lensing. The thermal lensing decreases the output laser beam quality and it mismatches the cavity and pump modes, which can lead to a lower laser output.

3.4.2 Experimental Setup

A schematic of the CW Alexandrite laser cavity pumped by a CW 532 nm diffraction limited Nd:YVO_4 green source (Finesse, Laser Quantum) is shown in Figure 3.8. In this design the oscillator shown in Figure 3.1 was modified such a way that its output laser spot size was sensitive to thermal lens variations in the crystal. Also, a 3 mm × 5mm × 7 mm Alexandrite crystal slab (NG Synoptics) doped with 0.155% of Cr^{3+} was held in an Aluminum crystal holder and was not actively cooled. The crystal was mounted on an xyz translation stage which helped to optimize its position with respect to the pump and cavity mode foci. The crystal was pumped with up to 6 W of CW green laser radiation at 532 nm. The pump had a low divergence TEM_{00} spatial mode and was focused into a ~45 μm spot size diameter inside the Alexandrite crystal by a 150 mm focal length lens. About 83% of the pump power was absorbed inside the crystal. The flat end mirror was an output coupler (OC) with 5% transmission. For thermal lens determination, a beam profiler was used to measure the infrared laser spot size that passed through a 150 mm focal length lens placed after 348 mm from the OC. The measurements were done from 1.5 W to 6 W of pump power at 10 different points. To eliminate the pump light, a 532 nm filter was placed after the OC. The thermal lens measurement setup is shown in Figure 3.8(b).

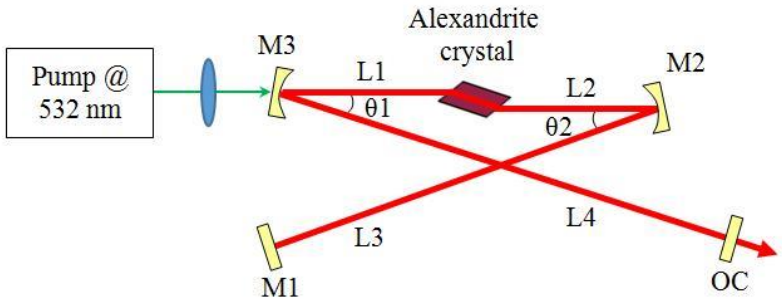

(a)

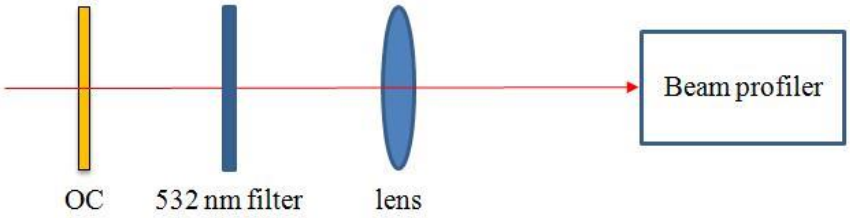

(b)

(c)

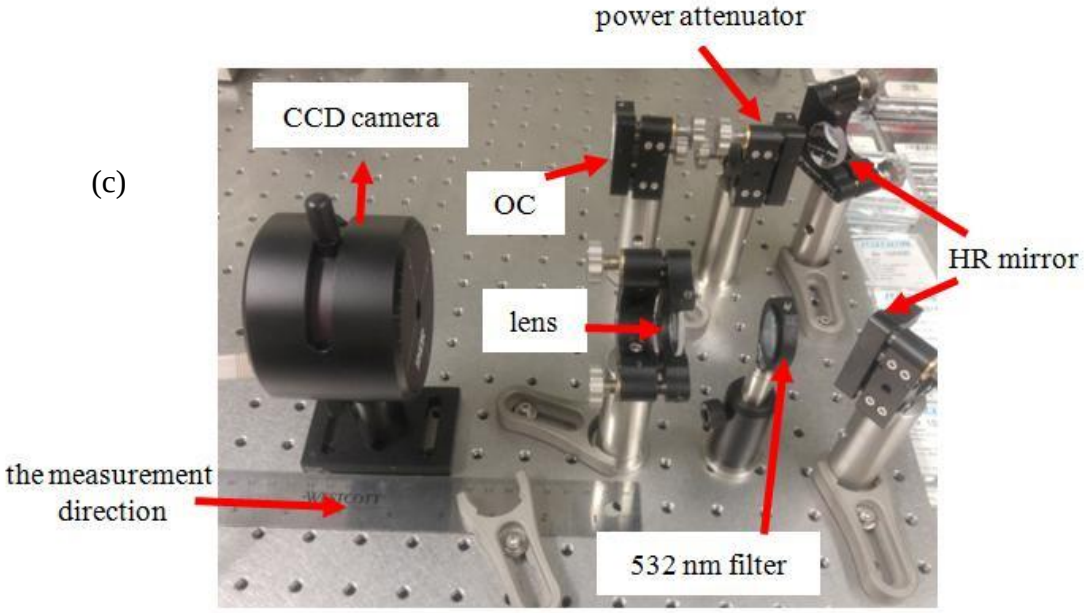

Figure 3.8. (a) Schematic of the CW Alexandrite laser. M1 is an HR flat mirror. M2 and M3 are the HR concave mirrors. OC is the output coupler. L1 = 53 mm, L2 = 48.5 mm, L3 = 802 mm, L4 = 702 mm, θ1 = θ2 = 9°. (b) Setup for the thermal lens measurement. (c) Photo of the measurement setup.

The beam waists of the laser were measured at different powers at the focal plane of the lens (f = 150 mm) by the beam profiler. Then, using the LASCAD resonator software, a virtual lens was added inside the crystal. When the simulation results and the experimental results matched, the virtual lens equaled the value of the thermal lens.

3.4.3 Results and Discussion

In this experiment Alexandrite laser operated at 750.9 nm which is shown in Figure 3.9. Consequently, as described by equation (3.1), the quantum defect of Alexandrite with 532 nm pump configuration is about 30%, which is relatively high. The measured Alexandrite output power versus pump power is demonstrated in Figure 3.10 which shows 22.85% slope efficiency and 18.5% optical to optical efficiency. Also, the laser output beam shapes at 1 W and 6 W of pump power showed in this figure demonstrate that the beam shape transformed from circular to elliptical. The corresponding beam quality factor (M^2) was obtained by fitting the data with Gaussian beam propagation equation (3.2). After the output coupler, a lens with f = 150 mm was used to focus the beam, and the averaged radii of the beam were measured for various locations after the lens by a beam profiler. Equation (3.2) describes the Gaussian beam waist taking into account a beam quality factor M^2 [1]:

$$w = w_0 \sqrt{1 + \left(\frac{\lambda_c M^2 (z - z_0)}{\pi w_0^2} \right)^2} \tag{3.2}$$

In this equation, z is the position of the measured beam radius w, w_0 is the beam waist radius, z_0 is the position of the beam waist and λ_c is the laser wavelength. By fitting equation (3.2) to the measured data, w_0 and M^2 were found. The fitting curves for the measured output power with

6 W of pump power are presented in Figure 3.11. The M^2 values in the horizontal and vertical directions for different pump powers are shown in Figure 3.12.

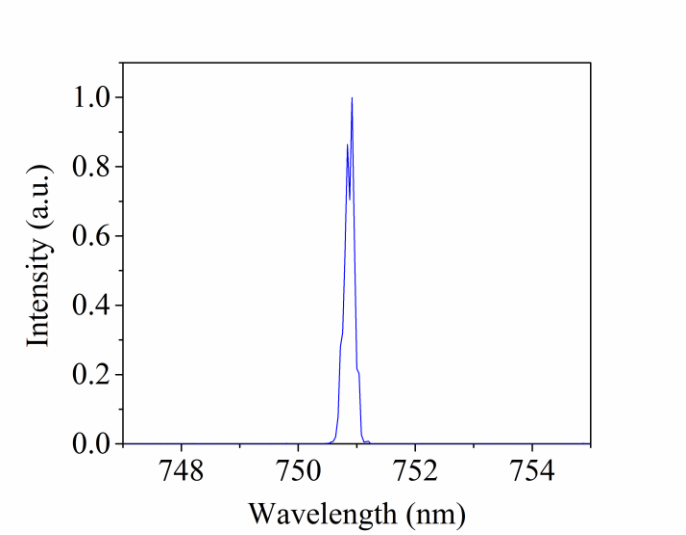

Figure 3.9. Alexandrite laser spectrum.

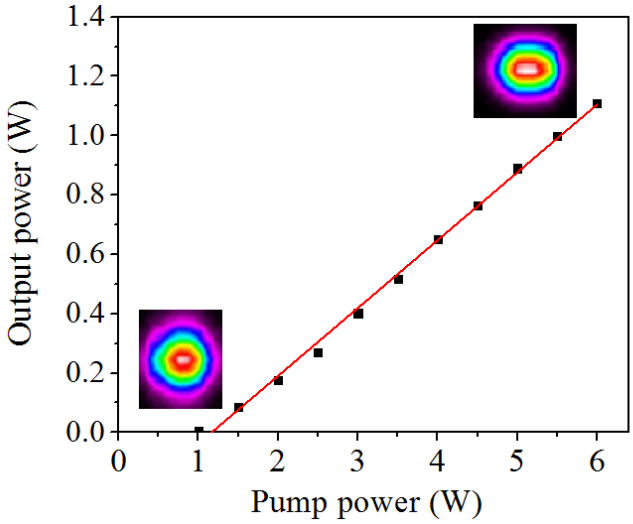

Figure 3.10. Alexandrite output power versus pump power.

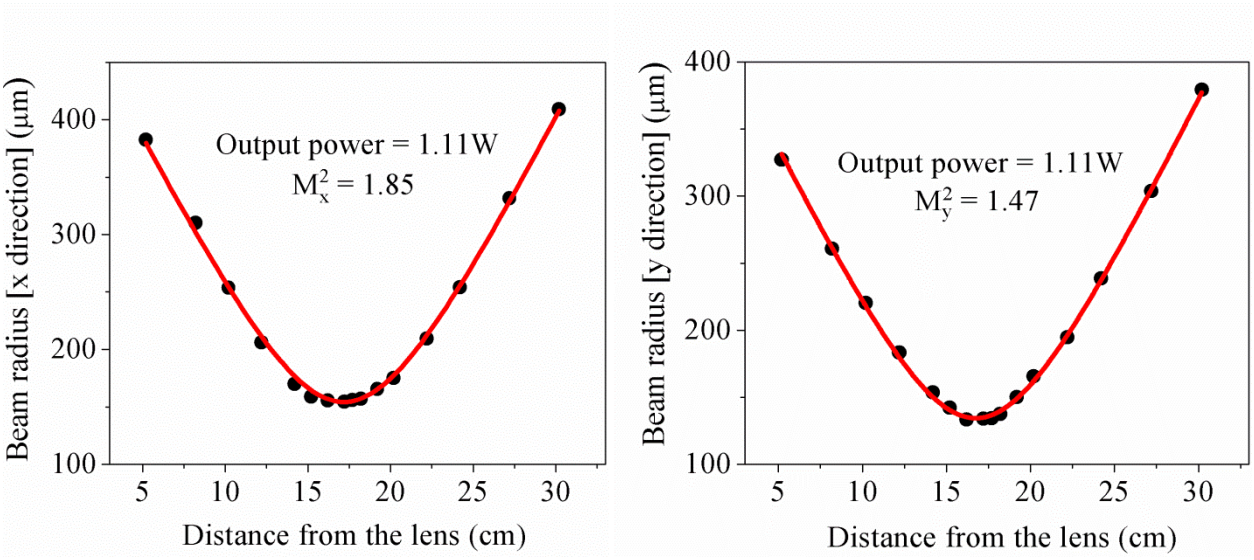

(a) (b)

Figure 3.11. Laser output beam quality M^2 at 6 W pump power in (a) horizontal [x] and (b) vertical [y] axis. The solid lines are the fitted curves.

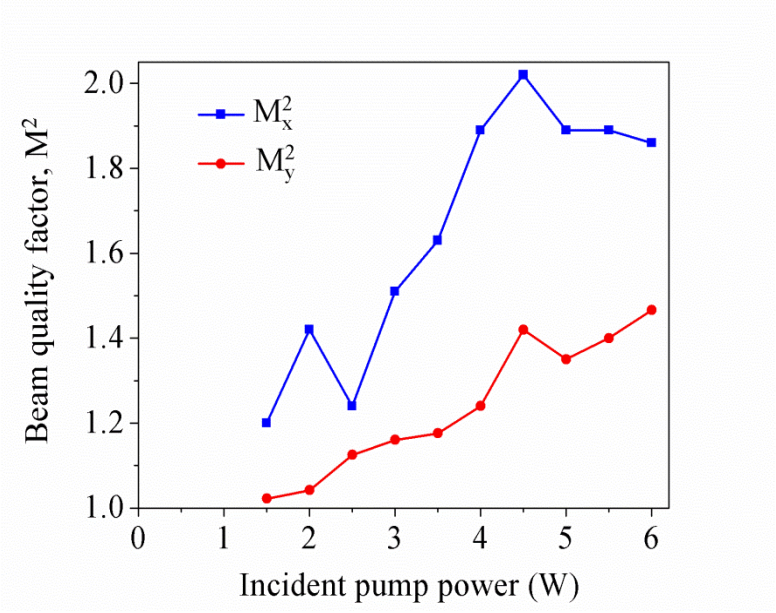

Figure 3.12. Beam quality values versus incident pump power (horizontal and vertical)

The focal lengths of the induced thermal lenses were then calculated using the LASCAD software that is based on ABCD matrix analysis. As a result, the focal length of thermal lens was determined to be 114 mm for the horizontal and 83 mm for the vertical direction at maximum output power. The focal lengths at different absorbed pump powers are presented in Figure 3.13. The results of the calculated optical power (inversed focal length taken in meters) of the measured thermal lens are shown in Figure 3.14.

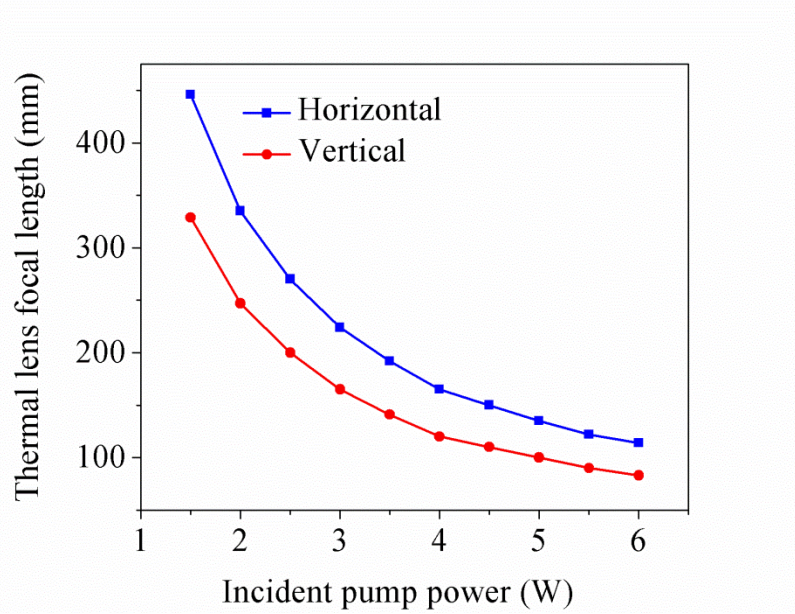

Figure 3.13. Focal length of the thermal lens in vertical and horizontal directions.

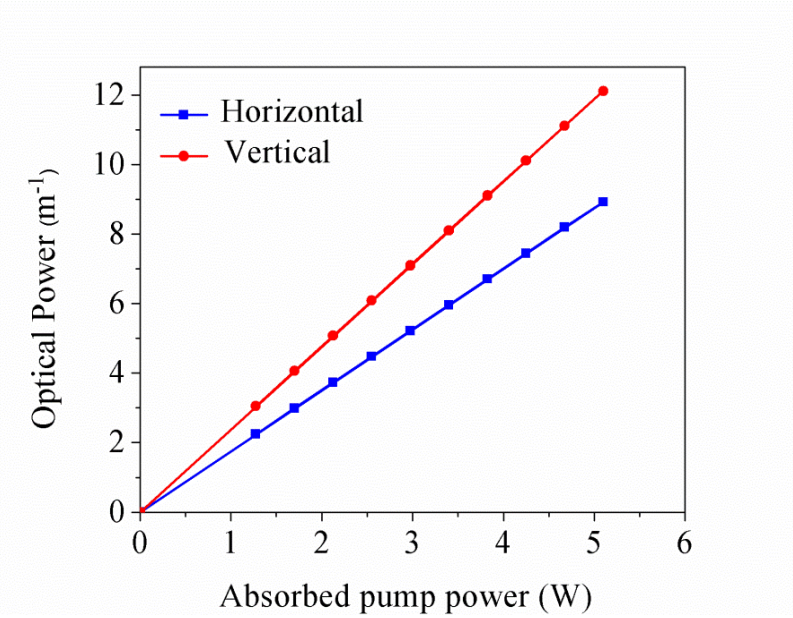

Figure 3.14. Optical power of the thermal lens in vertical and horizontal directions.

3.5 Conclusion

A high power broadly tunable operation of Alexandrite laser pumped at 532 nm was demonstrated. The laser produced up to 2.6 W of output power in a free running CW regime. This is the highest output power achieved to date in a high brightness laser-pumped configuration. A slope efficiency of 26% was achieved with a slight multimode output. The output wavelength was tunable from 715 to 800 nm with a FWHM of 58 nm. Also, a single transverse mode output with 1.24 W and slope efficiency of 29% was achieved. Due to the excellent thermo-mechanical properties of Alexandrite further power scaling is possible by heating the crystal to increase its stimulated emission cross section and/or by using an even higher pump power. The results obtained in this experiment can lead to the development of high power tunable sources of UV radiation and ultrafast mode-locked Alexandrite lasers.

Furthermore, studies of thermal lensing in Alexandrite lasers with maximum output power of 1.11 W were performed for the first time. The focal length of the thermal lens was experimentally determined to be 114 mm for the horizontal and 83 mm for the vertical direction at maximum output power. These results show that Alexandrite has a positive thermal lensing effect, and to obtain an efficient Alexandrite laser operation, the design of the laser oscillator needs to take into account the effect of thermal lensing. In addition, when developing the CW laser oscillator, the dual-wavelength operation of the CW laser oscillator was observed and will be investigated in the next chapter since this can be beneficial for further developing of laser technology.

Chapter 4: High Power Continuous-Wave Dual-Wavelength Alexandrite Laser

Dual-wavelength lasers are lasers that emit simultaneously two different wavelengths. In this chapter a high power dual-wavelength Alexandrite laser using a single plate birefringent filter (BRF) is demonstrated. When a 6 mm thick BRF was used, dual-wavelength output at 745.2 nm and 756.2 nm (5.9 THz of frequency difference) with 850 mW of average output power was achieved with 16.8% of optical-to-optical and 24.2% of slope efficiency. The tunability of dual-wavelength separation was also demonstrated by employing the 4 mm and 2 mm thick BRFs with similar output powers. To the best of our knowledge, this is the first demonstration of a dual-wavelength Alexandrite laser.

Laser active media with broadband gain are widely employed for the generation of ultrashort pulses. Another important aspect of broadband gain is that it offers a possibility to produce dual-wavelength output with terahertz (THz) frequency offset [45-48] which can be used to generate THz radiation. In recent research studies, THz waves have been used in attractive developing fields such as spectroscopy, imaging, communications, signal processing, and quantum information [49]. At present, THz radiation can be obtained by dipole antennas, free-electron lasers, and quantum-cascade lasers [48-50]. All of these techniques have disadvantages. For instance, broad-band radiation which is achieved with microwave lamps is not coherent. Additionally, although free-electron lasers can radiate in broad spectral range with great output power, they are not easily accessible because of their high price. On the other hand, however, one possible solution to these problems is the photo mixing of a dual-wavelength laser output on a compact and inexpensive dipole antenna [48]. One well-known way to achieve this phenomenon

is to use two Ti:sapphire lasers because of their high output power and large spectral range [50]. At the same time, in order to have a simple optical alignment and higher efficiency for THz generation, a single laser that provides collinear two-color output is preferable [47, 48]. Unfortunately, Ti:sapphire lasers are inefficient and costly. As an alternative, Alexandrite laser crystal has similar properties to the Ti:sapphire as explained in Chapter 2 and has been a recent topic of active research [51-53].

Alexandrite also has a broad wavelength tuning range from 700 to 820 nm [27, 28] as discussed in Chapter 2 which is well suited for simultaneous generation of multiple wavelengths. In general, the continuous-wave (CW) dual-wavelength lasing operation has been obtained with various methods, such as a double-prism-dispersion cavity [54], a multiple-plate birefringent filter (BRF) as the tuning element [55], two independent injection seeds [56], and controlling dual-wavelengths by the acousto-optic tunable filter [57]. Recently, a single plate BRF was effectively used with a broadband Yb:KGW crystal [58-60] to produce a dual-wavelength output in a simple and compact setup [46]. Due to the broadband spectral gain of Alexandrite this method is very attractive for the production of CW dual-wavelength radiation at around 750 nm. In this chapter, a dual-wavelength Alexandrite laser using a single BRF plate is demonstrated. To the best of our knowledge, this is the first report of dual-wavelength operation of an Alexandrite laser.

4.1 The Dual-Wavelength Laser Concept

Dual-wavelength operation of a laser is possible when the gain at both wavelengths exceeds the loss [46, 55, 61]. This condition can be realized owing to the broad emission spectrum of Alexandrite crystal and a wavelength-dependent loss mechanism which can equalize the gain. The

measured fluorescence spectrum of Alexandrite is shown in Figure 4.1. As can be seen, it can support broadband wavelength tuning as discussed in Chapter 2.

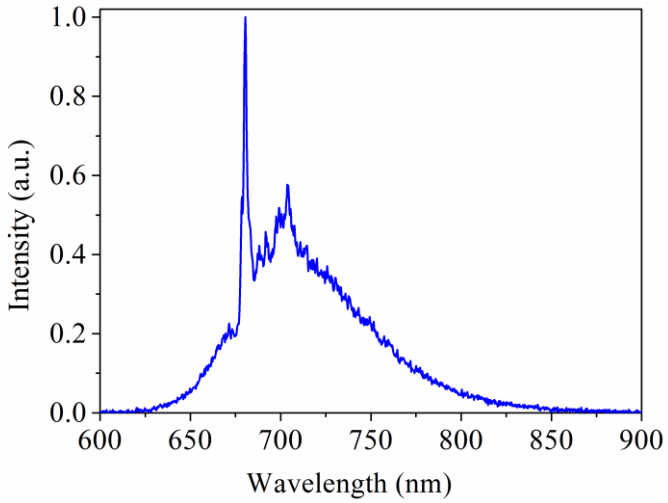

Figure 4.1. Spontaneous fluorescence spectrum of Alexandrite crystal. Vertical axis (a.u.).

One simple approach to introduce a wavelength-dependent loss is to employ a BRF [46, 55, 62]. The birefringence of this element causes a phase shift between the two orthogonal polarized components of the propagating light which manifests in the rotation of its original polarization. When a BRF is placed at Brewster's angle of incidence in a cavity, any rotation of polarization results in a periodic wavelength-dependent transmission profile (i.e. rejection of the produced *s*-polarized component). The low loss peaks happen at wavelengths with separation governed by the thickness of the filter. The free spectral range of a BRF (i.e. separation of the two low-loss wavelengths) can be expressed as equation (4.1) [63]:

$$\Delta\lambda = \frac{\lambda_0^2}{(n_e - n_o)d'} \tag{4.1}$$

where (n_e–n_o) is the difference between the extraordinary and ordinary refractive indices (~0.009 [64]), λ_0 is the peak lasing wavelength (~750 nm for an Alexandrite laser). The *d'*, which can be calculated using the equation (4.2), is the path length of light in the BRF oriented at Brewster's angle. For a quartz BRF with thickness *d*, Brewster's angle θ_B is 56.98° at 750 nm.

$$d' = d\cos(\sin^{-1}(\frac{\sin\theta_B}{n_o}))\cdot \tag{4.2}$$

Therefore, by rotating the BRF around the axis normal to its surface (i.e. changing the degree of polarization rotation of the incident light), the lasing wavelength can be tuned within the bandwidth of the gain, and when the adjacent wavelengths face the same loss, dual-wavelength operation can be achieved [46, 63, 64]. Furthermore, since the free spectral range of a BRF is inversely proportional to its thickness (see equation (4.1)), this allows one to control the wavelength separation by changing the thickness of a plate. It can also be shown that the linewidth of the generated wavelengths has the same dependence on the BRF thickness as the free spectral range [65].

4.2 Experimental Setup

The experimental setup is shown in Figure 4.2 and consisted of a standard Z-cavity configuration pumped with up to 5 W of CW green laser radiation at 532 nm (Finesse, Laser Quantum). The pump beam radiation was horizontally polarized (frequency-doubled Nd-ion laser) and was diffraction-limited. About 85% of the pump power was absorbed in the crystal. An Alexandrite crystal 7 mm long and doped with 0.155 wt.% of Cr^{3+} was Brewster-cut to provide polarized laser radiation with an E||b-axis (NG Synoptics). The crystal was held in an aluminum crystal holder at room temperature and was not actively cooled. The radii of curvature of the two

cavity focusing mirrors were 10 cm. Their folding angles were set to 9° to minimize the astigmatism. The pump had a low divergence TEM_{00} spatial mode and was focused by a 150 mm focal length lens into a ~44 μm diameter spot size inside the Alexandrite crystal. The designed cavity provided a good overlap between the pump and cavity modes. About 85% of the incident pump power was absorbed in the crystal. The transmission of the output-coupler (OC in figure 4.2) was 5% at 750 nm. A single plate BRF was placed in the resonator at Brewster's angle. Three BRFs with thicknesses of 6 mm, 4 mm and 2 mm were used to produce the dual-wavelength laser operation.

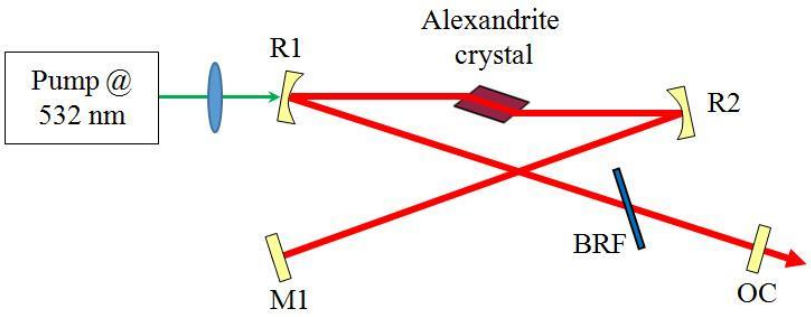

Figure 4.2. Schematic of the CW dual-wavelength Alexandrite laser. M1 is a highly reflecting flat mirror. OC is the output coupler.

4.3 Results and Discussion

In a free-running CW regime (without the BRF in the cavity) the laser oscillated at a peak wavelength of 755 nm with a linewidth of a few nm [42]. When a 6 mm thick BRF was introduced at Brewster's angle, the spectrum was narrowed down to 0.3 nm. The spectrum was measured with an optical spectrum analyzer which had a resolution of 0.07 nm. By rotating the BRF, a series of repeating spectra was achieved. A typical evolution of spectrum is demonstrated in figure 4.3,

where α denotes the relative BRF angle of rotation. Initially ($\alpha_1 = 0^o$), a single peak at 745.2 nm was observed. By rotating the BRF by 1 degree, the single peak moved to 748.5 nm. As the BRF was rotated further, the wavelength of the single peak changed until it reached 756.2 nm. By rotating the BRF by 0.5 degrees (α_6), the dual-wavelength regime was observed with a strong peak at 756.2 nm and a weak one at 745.2 nm. As the angle of the BRF was again changed by 0.5 degrees (α_7), the ratio of dual-wavelength peaks was changed to about an equal value. After rotating the BRF by another 0.5 degrees (α_8), the ratio of the peaks was changed further resulting in a weak signal at 756.2 nm and a strong one at 745.2 nm. Rotation of the BRF by an additional 0.5 degrees (α_9) transformed the dual-wavelength operation into a single wavelength one that peaked at 745.2 nm. Further rotation of the BRF led to the repetition of the spectral evolution.

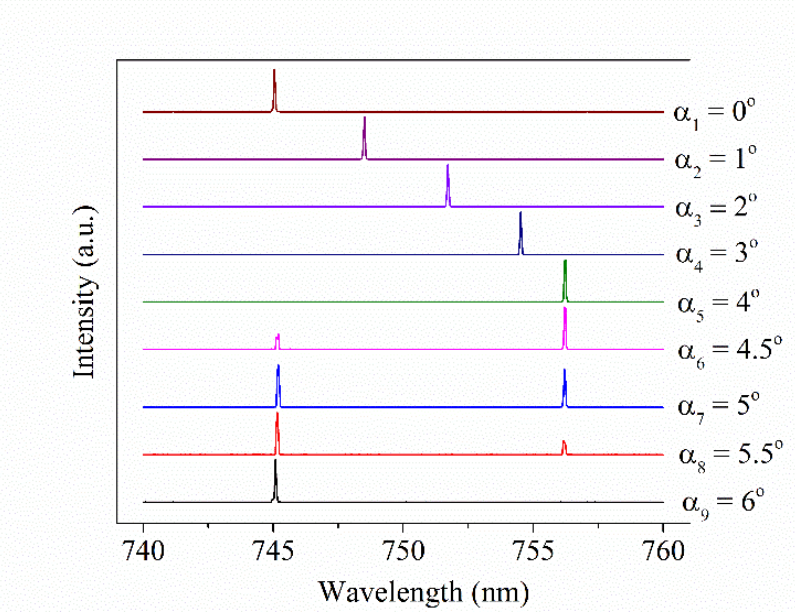

Figure 4.3. Typical sequence of Alexandrite dual-wavelength spectra when 6-mm-thick BRF is rotated around its axis. The spectral evolution starts from α_1 and continues until α_8. Then it repeats again starting from α_9.

The maximum output power of 850 mW was reached in a dual-wavelength regime at 745.2 nm and 756.2 nm. Each wavelength had a 0.3 nm linewidth and was horizontally polarized (*E*||*b*-axis). The measured CW dual-wavelength output power versus the pump power is shown in figure 4.4. This corresponded to a slope efficiency of 20.6% and an optical-to-optical efficiency of 16.8% with respect to the incident pump power. The slope efficiency with respect to the absorbed pump power was 24.2%. A transverse mode with beam quality factors of $M^2_X = 2.3$ and $M^2_Y = 1.5$ at the maximum output power of 850 mW is shown in the inset. The slight deviation from diffraction limited operation was probably caused by the thermal lensing which can reduce overlap between the pump and laser modes [66-68]. The CW dual-wavelength laser spectra for the maximum output power are illustrated in figure 4.5. The spectral intensity fluctuation was ~50% of their amplitudes (Figure 4.5(b) and (c)) while the output power fluctuated only by about 10 mW. The ratio of the peaks could be changed by rotating the BRF. The dual-wavelength regime could usually be achieved above the 3W of the pump.

In addition to 5% output coupler, OCs with 8% and 3% transmissions were used in the experiments. Among these OCs, the one with a 3% transmission demonstrated the best stability of dual-wavelength spectral amplitudes for the 6 mm thick BRF, which was ~20%. In this case, the average output power of the dual-wavelength regime with 5 W of pump power was 820 mW (with a fluctuation of 5 mW).

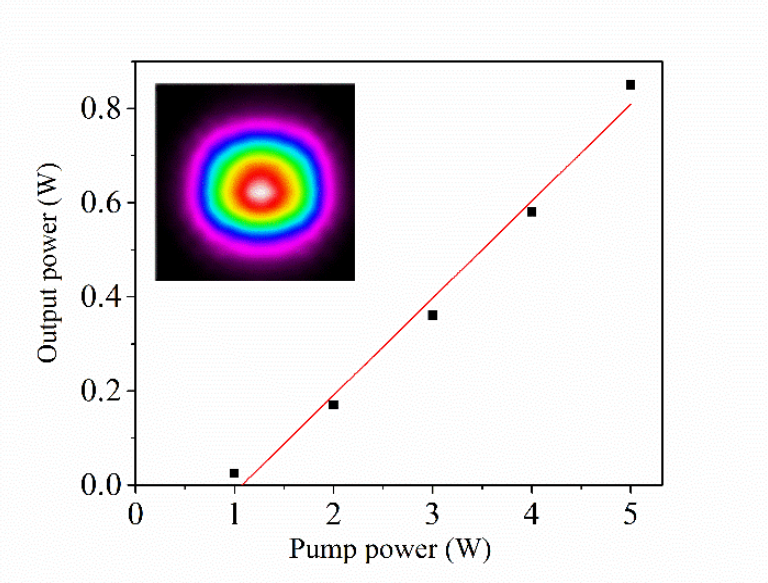

Figure 4.4. Alexandrite dual-wavelength output power versus pump power for 6 mm BRF and 5% OC. Inset: transverse beam intensity profile.

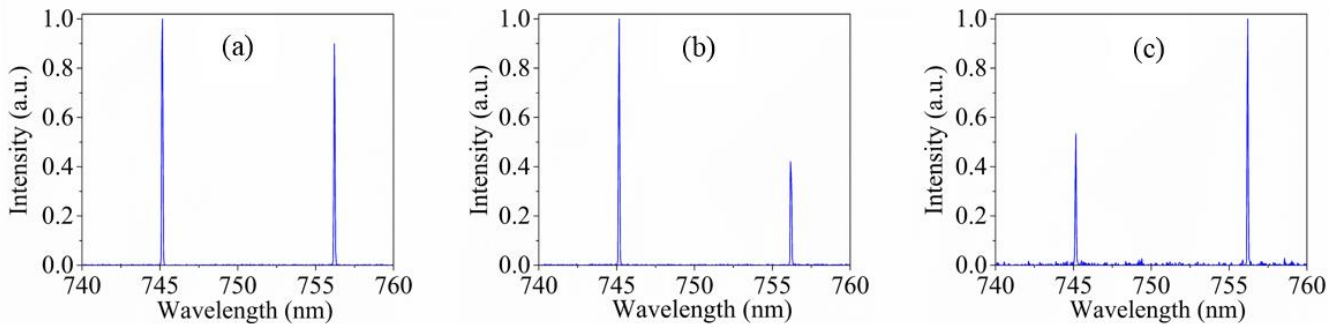

Figure 4.5. Alexandrite laser spectrum at 5W of pump power using 6 mm-thick BRF. (a) Equal peaks when the gain and loss are the same between the two wavelengths (b) and (c) fluctuating 50% between amplitudes of two wavelengths.

Similar experiments were conducted for the 4 mm and 2 mm thick BRFs. The best performance in terms of power was recorded with a 5% OC. The dual-wavelength performance of

the laser and spectral behavior was similar to that with the 6 mm thick BRF. In case of the 4 mm (2 mm) BRF the maximum output power reached 870 mW (765 mW) with the wavelengths pair at 744.2 nm and 757.2 nm (733.8 nm and 759 nm). Each wavelength had a 0.4 nm (0.5 nm) linewidth with about 3 nm (5 nm) wavelength tunability. The slope efficiency was measured to be 21% (18.8%) and the optical-to-optical efficiency was 17.4% (15.3%). The spectral fluctuations of the dual-wavelength amplitudes were 60% (70%). In each case the laser beam quality factors were measured to be $M^2_X = 2.1$ and $M^2_Y = 1.6$ ($M^2_X = 2.3$ and $M^2_Y = 1.8$).

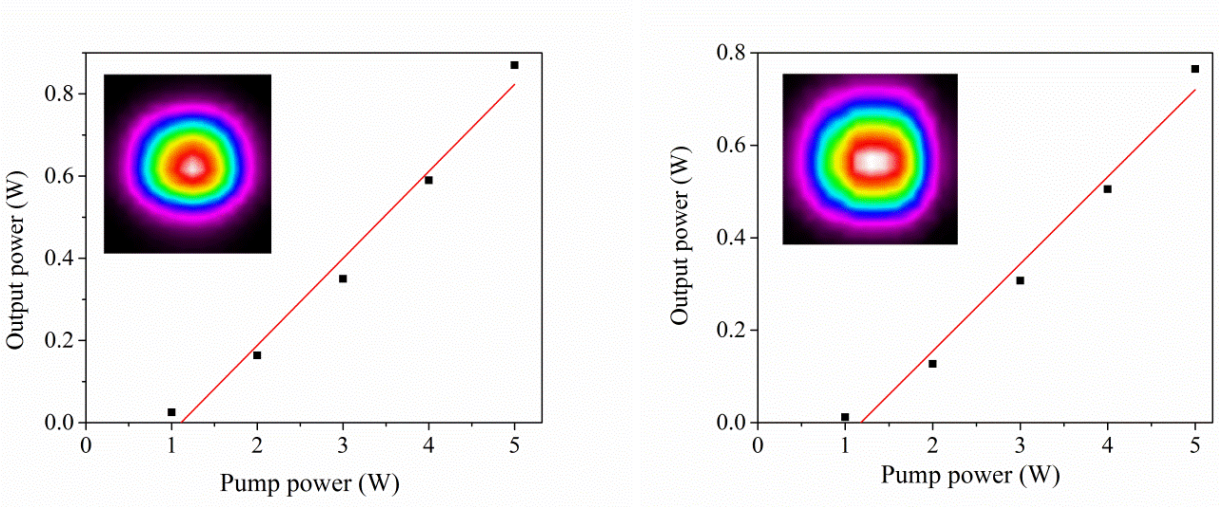

Figure 4.6. Alexandrite dual-wavelength output power versus pump power with 5% OC for (a) 4 mm BRF and (b) 2 mm BRF. Inset: transverse beam intensity profile.

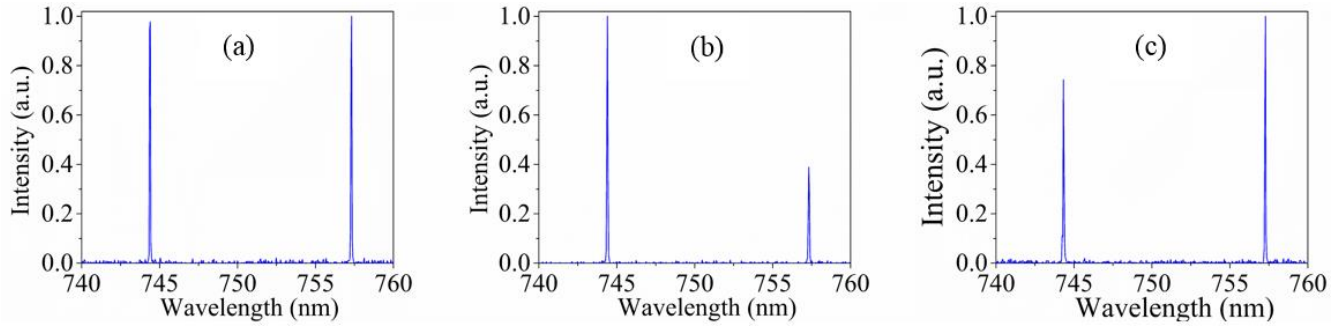

Figure 4.7. Alexandrite laser spectrum at 5W of pump power using 4 mm-thick BRF. (a) Equal peaks when the gain and loss are the same between the two wavelengths (b) and (c) fluctuating 60% between amplitudes of two wavelengths.

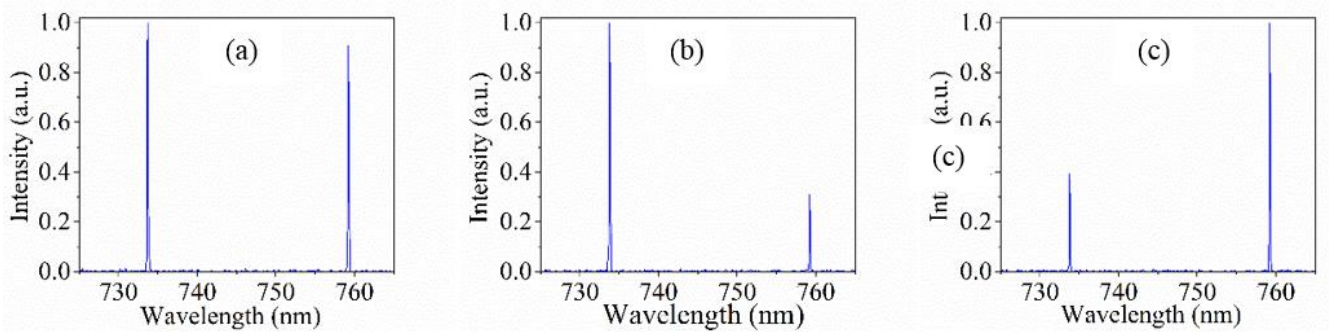

Figure 4.8. Alexandrite laser spectrum at 5W of pump power using 2 mm-thick BRF. (a) Equal peaks when the gain and loss are the same between the two wavelengths (b) and (c) fluctuating 70% between amplitudes of two wavelengths.

Table 4.1. Summary of dual-wavelength operation results for different BRFs.

BRF (mm)	λ_1 (nm)	λ_2 (nm)	$\Delta\lambda_{exp}$ (nm)	$\Delta\lambda_{th}$ (nm)	$\Delta\lambda_{lw}$ (nm)	$\Delta\nu$ (THz)	M^2_X	M^2_Y	η (%)	η_{abs} (%)	η_{op} (%)	P_{out} (mW)
6	745.2	756.2	11.0	8.7	0.3	5.9	2.3	1.5	20.6	24.2	16.8	850
4	744.2	757.2	13.0	13.0	0.4	6.9	2.1	1.6	21	24.9	17.4	870
2	733.8	759.0	25.2	26.0	0.5	13.6	2.3	1.8	18.8	22.2	15.3	765

Table 4.1 summarizes the results of the experiments, where λ_1 and λ_2 are the two generated wavelengths, $\Delta\lambda_{exp}$ and $\Delta\lambda_{th}$ are the experimental and theoretical wavelength separation, $\Delta\lambda_{lw}$ is the linewidth at half maximum, $\Delta\nu$ is the frequency difference between the two wavelengths, M^2_X and M^2_y are the laser beam quality factors in the horizontal (x) and vertical (y) directions, η is the slope efficiency with respect to the incident pump power, η_{abs} is the slope efficiency with respect to the absorbed pump power, η_{opt} is the optical-to-optical slope efficiency, and P_{out} is the output power. The results show that the separation of the generated wavelengths decreased as the thickness of the used BRF was increased, which agreed well with calculations using equation (4.1). The measured linewidths also exhibited the same trend.

4.4 Conclusion

In conclusion, a 532 nm green pumped continuous-wave, dual-wavelength Alexandrite laser using a single plate BRF (with 6 mm, 4 mm and 2 mm thicknesses) was demonstrated. With 5 W of pump power, the laser produced up to 870 mW of output power with wavelength separation selectable between 11 nm and 25.2 nm (5.9–13.6 THz). The results show that Alexandrite coupled

with a single plate BRF is a viable source for producing dual-wavelength radiation, and if pumped with currently available red diode lasers [29, 31, 42], higher output power and optical efficiency can be expected.

In the next chapter, after a brief review of mode locking concept, the results of a quantum-dot semiconductor saturable absorber mode-locked Alexandrite laser will be presented.

Chapter 5: Femtosecond Alexandrite Laser Passively Mode-Locked By InP/InGaP Quantum-Dot Saturable Absorber

In this chapter an Alexandrite laser passively mode-locked using an InP/InGaP quantum-dot semiconductor saturable absorber mirror (QD-SESAM) is demonstrated. The laser was pumped at 532 nm and generated pulses as short as 380 fs at 775 nm with an average output power of 295 mW. To the best of our knowledge, this is the first report on a passively mode-locked femtosecond Alexandrite laser using a SESAM in general and a quantum-dot SESAM in particular. In this chapter, the principles of mode locking are described. Then, after a brief review of the previous results in the mode locking regime, the experimental set up and the results of mode-locked Alexandrite laser in this work are demonstrated.

5.1 Mode Locking

Mode locking is a technique used to produce ultrashort femtosecond pulses via loss modulation inside a cavity. This loss modulation can be passive or active, but passive mode locking can provide shorter pulses than active mode locking. As the number of longitudinal modes oscillating inside the cavity increases (due to faster loss modulation), pulses with shorter time duration can be obtained. This can be described by the Fourier transform theorem because when a function has larger bandwidth in frequency domain, it has narrower duration in time domain [1]. Passive loss modulation provided by Kerr-lens or saturable absorber helps to produce a fixed relationship between the phases of the oscillating longitudinal modes inside the cavity. Thus, all of the modes inside the cavity have constructive interference. All these processes are illustrated in Figure 5.1 [1].

In fact, several longitudinal modes with frequencies defined by equation (5.1) [1] are allowed to exist in a cavity with length L, where c is the speed of light and q is an integer number.

$$\nu = \frac{cq}{2L} \tag{5.1}$$

These longitudinal modes do not have a well-defined amplitude as well as phase relation in a free-running laser, so a series of unruly spikes are provided at the output due to a statistical average of all oscillating modes. On the other hand, longitudinal modes can have constructive and destructive interference with each other if they have a fixed phase shift. In this way, according to the number of existing modes in the cavity, a sequence of pulses with short time duration and high peak intensity could be obtained. In fact, the fixed relationship between the phases of longitudinal modes can be obtained by creating loss modulation in the laser oscillator. Figure 5.2(a) shows in a very short time when loss is lower than the laser gain, short pulses of light can be created. In Figure 5.2(b), the top diagram shows that the short pulses with high intensity are formed by providing identical phases between all of the modes of irregular spike series. The diagram in the bottom of Figure 5.2(b) shows the modes which have random phase shifts with respect to each other. The pulse width is inversely proportional to the number of modes oscillating in the cavity.

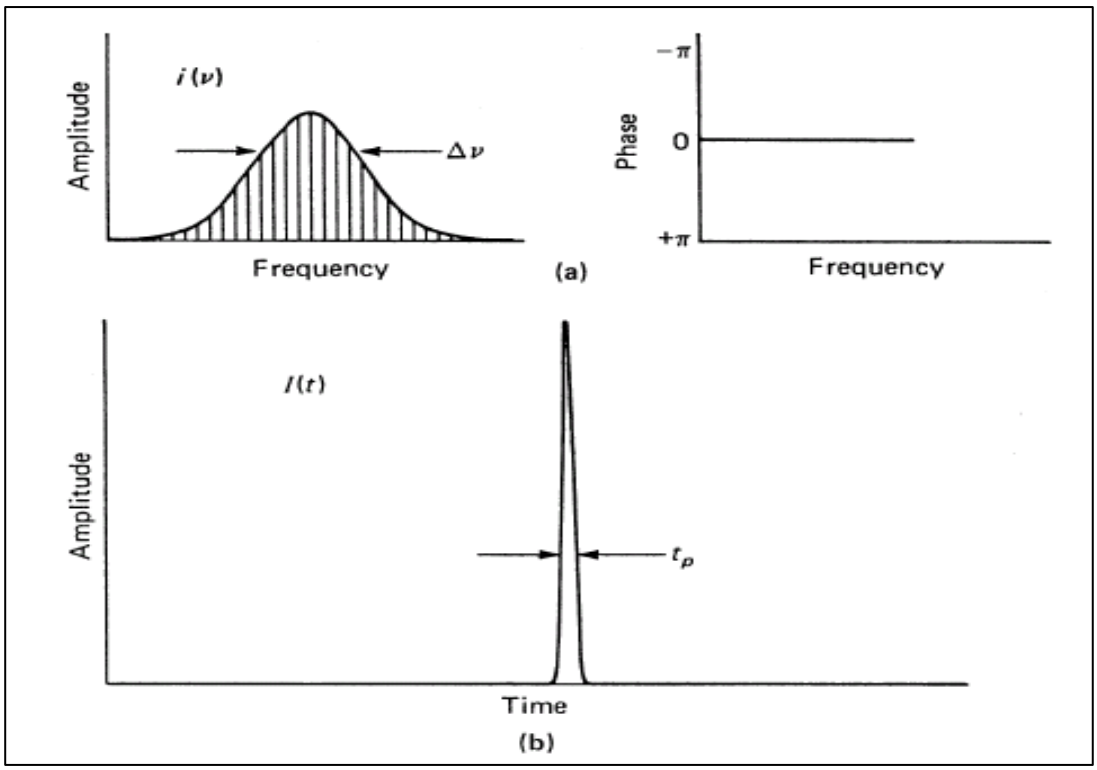

Figure 5.1. Short pulse produced by mode locking. (a) Amplitude of frequencies resonating inside the cavity has a Gaussian distribution, but all oscillating frequencies have the same phase. (b) In time domain the superposition of different frequency modes produces a short pulse. Used with the permission of Springer Nature [1].

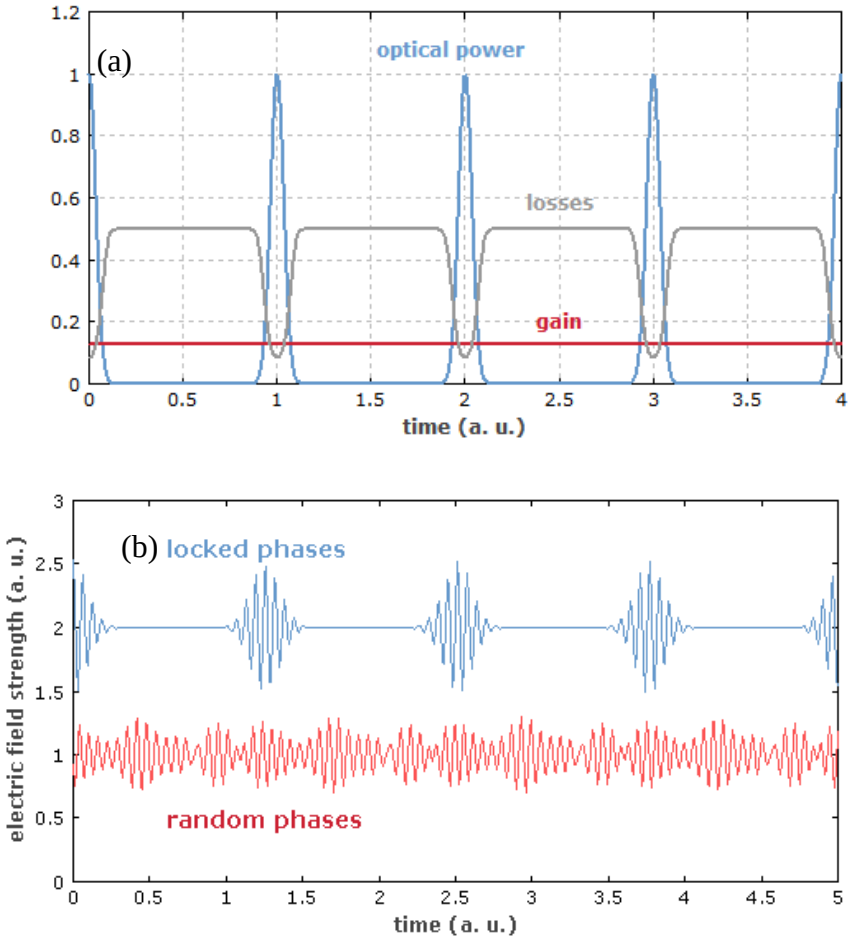

Figure 5.2. (a) Short pulses provided by loss modulation inside a cavity. Reproduced with permission [69]. (b) Temporal development of the intracavity field in a laser for a fixed phase relationship between the modes in mode locking provided from random phases by loss modulation. Reproduced with permission [70].

The two methods for mode locking are active mode locking and passive mode locking. In active mode locking the modes are locked in phase by using an active modulator to modulate the amplitude or the phase of the modes via periodic loss of light energy. In fact, the modulator amplifies the circulating energy with zero-loss while the rest of the energy is blocked from the gain. However, the pulse width achieved by active mode locking is limited because the modulator

cannot provide fast enough modulation to generate ultrashort pulses. Another method, passive mode locking, is favored. In this technique, a saturable absorber is used as a loss modulator that acts passively by using the short pulses themselves. The shorter the pulses, the faster the loss modulation is produced. Two of the most important passive mode locking techniques are Kerr-lens mode locking (KLM) and semiconductor saturable absorber mirror (SESAM) mode locking.

5.2 Passive Mode Locking of Alexandrite Laser with Saturable Dyes

Alexandrite has the ability to generate ultrashort pulses via the saturable absorber mode locking or Kerr-lens mode locking (KLM) techniques that were mentioned above. Up to now, DSI and DTTS organic saturable dye absorbers [35] have been used for passive mode locking of Alexandrite lasers. However, the shortest pulse duration achieved using a DSI organic saturable dye absorber was 8 ps (picosecond), with a 12.5 Hz repetition rate and a 1.1 W average output power at 750 nm with 80 J of pump energy [35].

Since DSI absorption spectrum included 750 nm line (the center of emission spectrum of Alexandrite), a special solution was used to shift its absorption spectrum to match the longer wavelength part of the Alexandrite emission spectrum. Another absorber, DTTS in ethanol, generated 90 picosecond pulses with the tuning range of 750-875 nm at room temperature. In these experiments, it was observed that by increasing the temperature, more gain could be achieved. However, higher temperatures (50^{o}C) caused an increased thermal lensing effect, so optical resonator modification was needed to compensate for a thermal lensing effect. In addition, increasing the active ion Cr^{3+} concentrations in the Alexandrite rod and using more pump energy has been shown to increase the output power and gain.

5.3 Semiconductor Saturable Absorber Mirror (SESAM)

In a saturable absorber which is typically an InGaAs or GaAs quantum-well, loss decreases as the intensity in the resonator growths. An integrated type of a saturable absorber and a Bragg reflector that acts as a mirror on a single wafer is called semiconductor saturable absorber mirror (SESAM). Bragg reflector is composed of different layers of low and high refractive index materials. High reflectance is produced when reflected waves at each layer strengthen each other due to the light interference. The structure of SESAM is shown in Figure 5.3 [71]. In fact, the Bragg mirror reflects high energy light that passed through the absorber. However, low energy light experiences loss. Indeed, as a pulse of light propagates through the SESAM the leading edge with low intensity would be absorbed because it is absorbed by electrons in the absorber layer thus causing them to move to higher energy states. Conversely, the powerful central part of the pulse would pass through the absorber almost unaffected because it saturates the absorber (i.e. there would be no more electrons left in lower energy state to absorb the light). The recovery of the absorber includes two steps which are a fast recovery time or fast loss modulation (several hundred femtoseconds) due to intraband thermalization followed by a slow recovery time (picoseconds or nanoseconds) due to interband recombination as illustrated in Figure 5.4. In this way, the fast edge of loss modulation is more effective in producing ultrashort pulses while the slow edge of loss modulation helps self-starting of mode locking. To produce shorter pulses, a faster loss modulation is required. Because different frequencies have different refractive indexes, lower frequencies propagate faster than higher frequencies, so pulses are chirped. By using the dispersion compensating devices in the cavity, the group delay between different frequency components can be removed. SESAM can produce femtosecond pulses and it can be used for triggering Kerr-lens mode locking to produce even shorter pulses [72, 73].

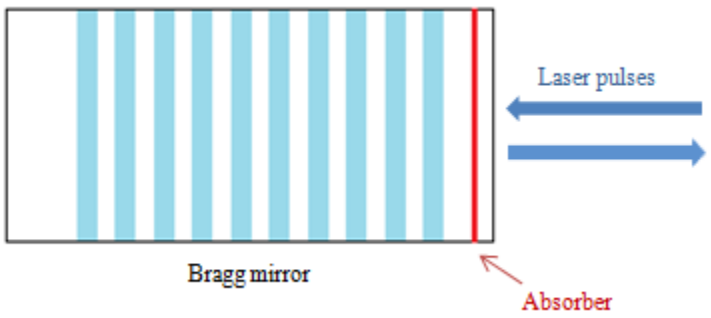

Figure 5.3 Typical structure of a semiconductor saturable absorber mirror.

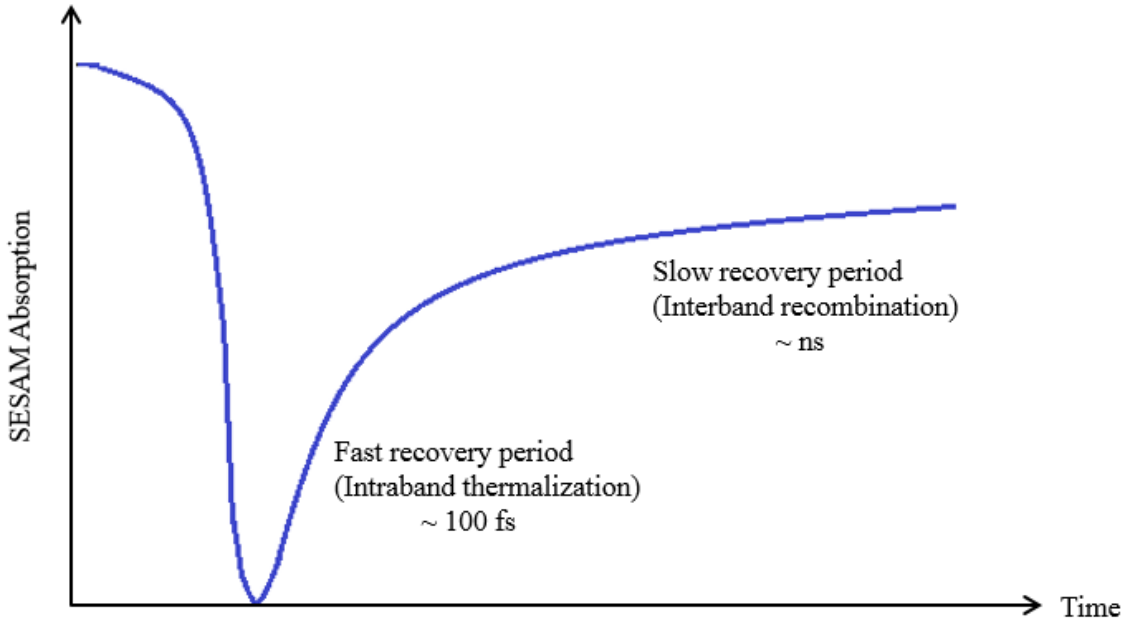

Figure 5.4 Recovery mechanism of the SESAM.

There are three important parameters of SESAM as showed in Figure 5.5 [72]. Saturation fluence, denoted as $F_{sat,A}$, is defined as a pulse fluence where the device absorption is reduced by 1/e of the initial value. Also, modulation depth, shown as ΔR, is another factor that shows the saturable part of nonlinear reflectivity. The other factor is non-saturable loss, denoted as ΔR_{ns}, which describes the remaining loss of the absorber once an intense pulse has bleached the device [72]. To obtain full modulation depth of the saturable absorber in CW mode-locked lasers, the

pulse energy should be approximately five times the absorber saturation fluence to bleach the absorber [74]. For avoiding Q-switching instabilities, condition (5.2) should be fulfilled [74]. $A_{eff,L}$ and $A_{eff,A}$ are the mode areas in a laser crystal and on SESAM, respectively. F_s is the saturation fluence of the laser crystal and $F_{P,A}$ is the pulse fluence on SESAM.

$$(F_{P,A})^2 > F_s \frac{A_{eff,L}}{A_{eff,A}} F_{sat,A} \Delta R \qquad (5.2)$$

When compared with Kerr-lens mode-locking, SESAM is slower and typically has lower modulation depth.

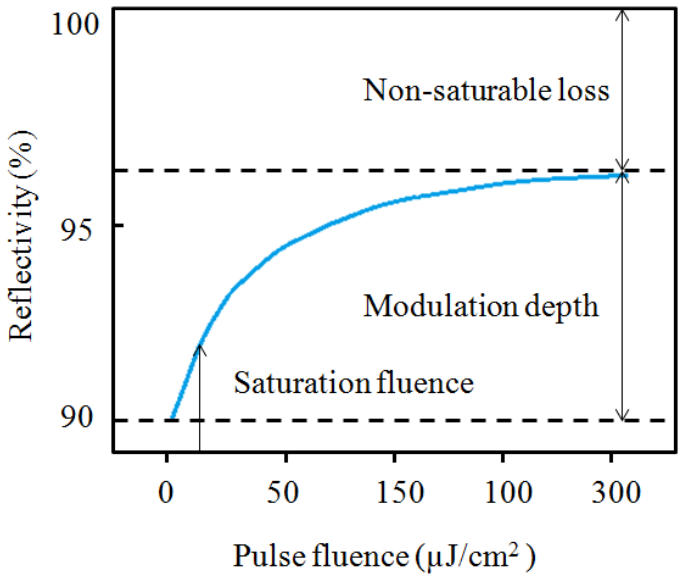

Figure 5.5. Nonlinear reflectivity as a function of incident pulse fluence on a typical SESAM that demonstrates saturable absorber parameters that are saturation fluence $F_{sat,A}$, modulation depth ΔR and nonsaturable loss ΔR_{ns}.

5.4 Quantum-Dot Semiconductor Saturable Absorber Mode-Locked Alexandrite Laser

Ultrafast laser sources in the near-infrared spectral region are highly desirable for a wide range of applications as described in Chapter 1. In fact, as it is explained in Chapter 1, Alexandrite can be an appropriate candidate to replace the widely used Ti:sapphire laser. At the same time, passive mode locking with a semiconductor saturable absorber mirror (SESAM) is an effective method that is widely used with Nd-doped [75-77] and Yb-doped [78-80] gain media to produce ultrashort pulses because it does not require critical cavity alignment that is needed in case of KLM lasers [81-83]. Therefore, the extension of SESAM mode locking to Alexandrite is a promising alternative. In this respect, quantum-dot SESAMs (QD-SESAMs), which can provide broadband absorption and emission spectra attributed to the inhomogeneous broadening associated with the size dispersion of QDs, are particularly attractive for generation of ultrashort pulses. It is worth mentioning that previous attempts of passive mode locking of Alexandrite using saturable dye absorbers could only produce picosecond (8-10 ps) pulses [35, 84]. On the other hand, recently SESAMs have been used for Q-switching of Alexandrite and produced 550 ns long pulses [85]. This chapter reports on the first passively mode-locked Alexandrite laser using an InP/InGaP QD-SESAM that produced femtosecond pulses as short as 380 fs at 775 nm with an output power of 295 mW and pulse repetition frequency of 79.9 MHz. The results of this work open the way for the development of efficient diode–pumped ultrashort pulse Alexandrite lasers that can rival the currently used Ti:sapphire lasers in many industrial, scientific and medical applications.

5.4.1 Experimental Setup

The experimental setup of the QD-SESAM mode-locked Alexandrite laser is schematically shown in Figure 5.6. The designed cavity is based on the oscillator used for the passive mode locking of a Ti:sapphire [86], and it consists of 5 mirrors. The Brewster-cut Alexandrite crystal was 7 mm in length and doped with 0.155% of Cr (NG Synoptics). The crystal was mounted on a translation stage which helped to optimize its position with respect to the pump and cavity mode foci. The crystal was pumped at 532 nm by a frequency-doubled Nd:YVO_4 laser with a maximum power of 7.3 W (Finesse, Laser Quantum). The pump was focused into a ~45 μm spot size diameter inside the crystal by a 150 mm focal length lens. About 85% of the pump power was absorbed in the crystal. Mirrors M1-M3 were highly reflecting (HR) in the 650-900 nm range. The Alexandrite crystal was placed between the two folding mirrors (M1 and M2) with 100 mm radii of curvature. The cavity contained the InP/InGaP QD-SESAM which was used as one of the plane end mirrors. Previously, the QD-SESAM used in this work was tested with Ti:sapphire lasers to produce picosecond pulses at 800 nm and had a non-saturable loss of ~1% [87]. The QD-SESAM samples were provided to us by Prof. E. Rafailov from Aston University, UK. In general, the QD-SESAMs were shown to offer low saturation fluence [87], controllable modulation depth [85] and broadband operating wavelength range [86-91]. An appropriate mode spot size on the QD-SESAM was obtained by using the focusing mirror M3 with the radius of curvature of 200 mm. The delta cavity geometry (see Figure 5.6) resulted in a spot size diameter of about 53 μm within the Alexandrite crystal and approximately 171 μm on the QD-SESAM. The effect of thermal lensing [67] was also considered in the cavity design. Two SF10 prisms (P1 and P2) separated by 345 mm were used to compensate for the positive intracavity dispersion. The output coupler (OC) had 3% transmission around 750 nm.

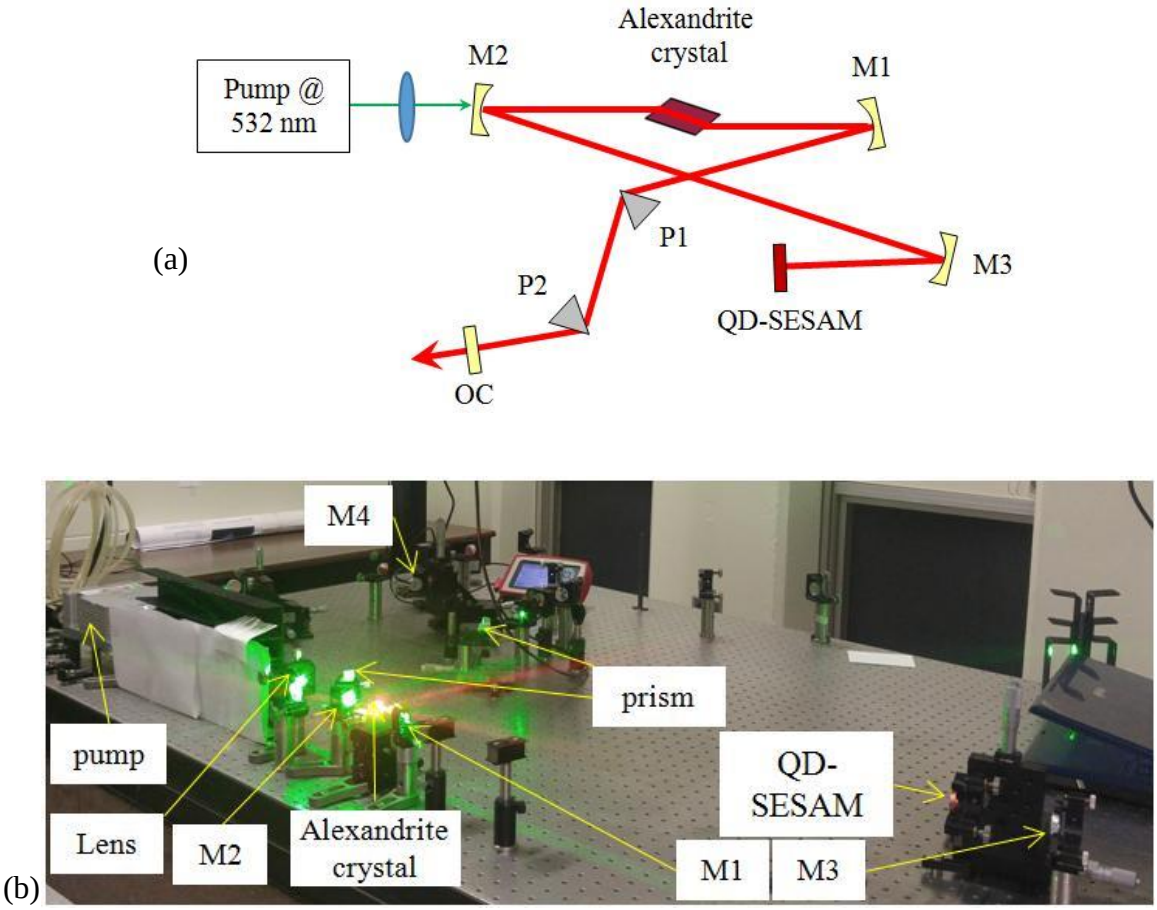

Figure 5.6. (a) Schematic of the QD-SESAM mode-locked Alexandrite laser. (b) A picture of the setup.

5.4.2 Results and Discussion

The mode-locked laser operation was initiated and sustained by the InP/InGaP QD-SESAM used as one of the end mirrors. The used QD-SESAM was originally designed for Ti:sapphire [87], so it shifted the Alexandrite emission wavelength from the typical 755 nm [28] to longer wavelengths. Reliable mode locking with an average output power of 325 mW at the incident pump power of 7.12 W was achieved. Pulses as short as 420 fs in duration were produced with 1.7 nm wide (FWHM, full width at half maximum) spectrum centered at 774 nm that indicated a time-bandwidth product of 0.359. The fluence on the saturable absorber was about 590 μJ/cm^2 and no

damage was observed. The autocorrelation trace of 420 fs pulses and the corresponding spectrum are displayed in Figure 5.7(a) and Figure 5.7(b), respectively. In addition, by optimizing the laser cavity alignment, pulses as short as 380 fs in duration with an average output power of 295 mW were produced at 7.3 W of an incident pump power. The spectrum was centered at 775 nm and had a FWHM bandwidth of 1.8 nm that resulted in a time-bandwidth product of 0.341. The fluence on the saturable absorber was about 535 $\mu J/cm^2$. The autocorrelation trace of the 380 fs pulses and the corresponding spectrum are displayed in Figure 5.8(a) and Figure 5.8(b), respectively. The radio frequency (RF) spectrum of the pulse train is shown in Figure. 5.9(a) and demonstrates high signal-to-noise ratio indicative of stable mode locking without Q-switched mode-locked instabilities. Furthermore, stable single-pulse mode locking and the absence of Q-switching instabilities were confirmed using a long scan range (200 ps) background-free intensity autocorrelator (Femtochrome, FR-103XL) and a fast oscilloscope/photodetector with photodiode that had a combined resolution of ~100 ps [4]. Considering the repetition rate of ~79.9 MHz, 420 fs laser pulses had energy of ~4.1 nJ and peak power of >9.5 kW. The shorter 380 fs laser pulses had energy of ~3.7 nJ and similar peak power. Optical-to-optical efficiency was 5.4% for the longer pulses and 4.8% for the shorter pulses with respect to the absorbed pump power. The transverse intensity profile of the beam in the mode-locked regimes is shown in Figure 5.9(b). The laser operated in the fundamental transverse mode. In both cases the laser threshold was at about 2.5 W and the mode locking threshold was approximately at 4.55 W of incident pump power. Multi-pulse oscillation was observed at higher than 7.12 W or 7.3 W of pump powers for longer and shorter pulses, respectively.

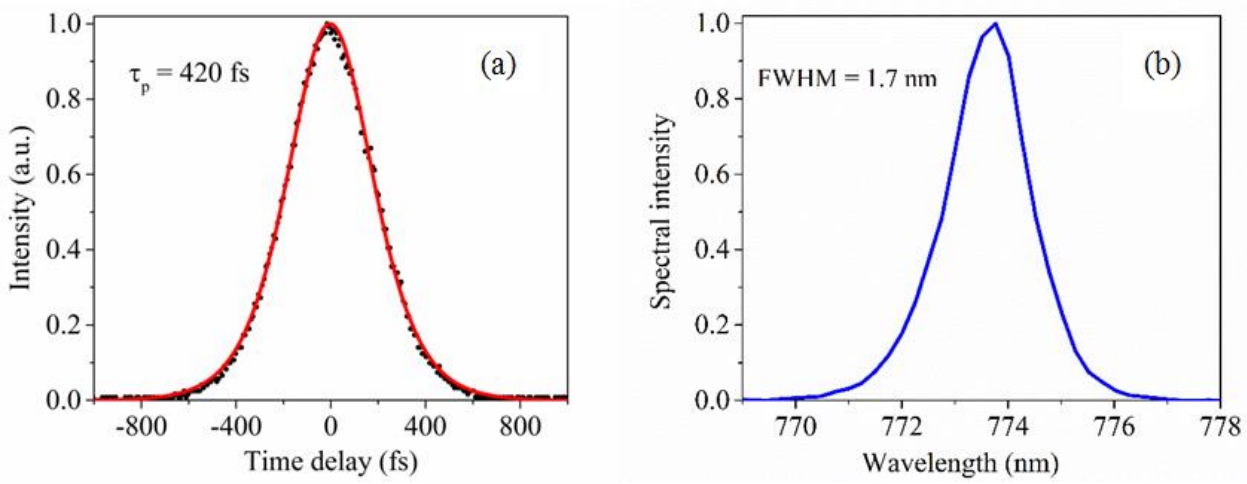

Figure 5.7. Measured (a) autocorrelation trace of 420 fs pulses with fit assuming a sech^2 intensity profile and (b) their spectrum.

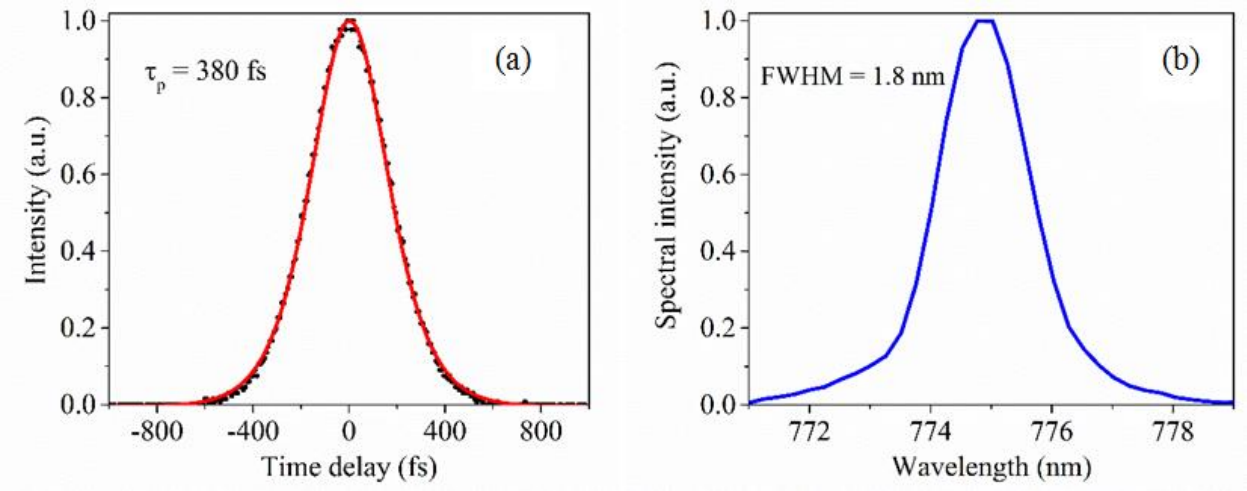

Figure 5.8. Measured (a) autocorrelation trace of 380 fs pulses with fit assuming a sech^2 intensity profile and (b) their spectrum.

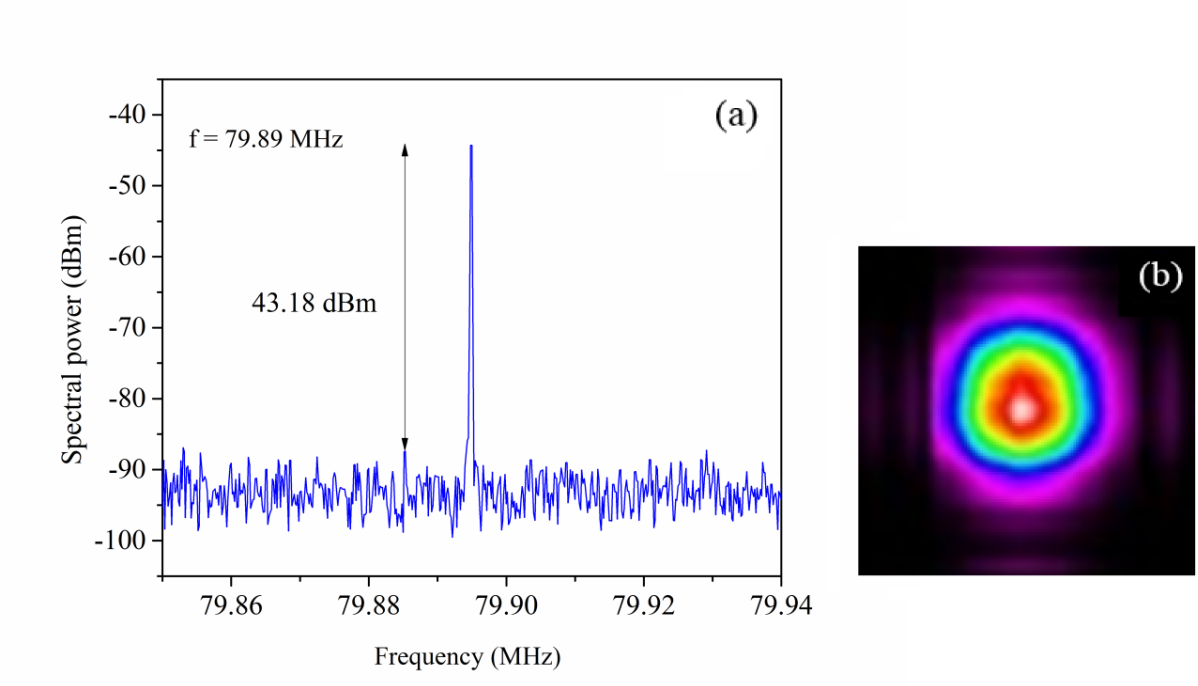

Figure 5.9. (a) RF spectrum of the 380 fs pulse train taken with resolution bandwidth of 1 kHz and (b) transverse beam intensity profile of the mode-locked laser.

5.5 Conclusion

A passively mode-locked Alexandrite laser using an InP/InGaP QD-SESAM was demonstrated for the first time. Pulses with duration as short as 380 fs and 420 fs with an average output power of 295 mW and 325 mW, respectively, were generated. The laser was pumped with up to 7.3 W at 532 nm and operated around 775 nm. To the best of our knowledge, this is the first report of a passively mode-locked Alexandrite laser using a SESAM in general and a quantum-dot SESAM in particular. Due to the broad tuning range (~85 nm) of Alexandrite [28], a careful dispersion management [52] should lead to the generation of even shorter pulses. In addition, more efficient mode locking should be possible by designing QD-SESAMs specifically for Alexandrite

laser crystal that has a gain peak around 755 nm wavelength [26, 27]. Also, low quantum defect of visible diode pumping [29, 30] should lead to efficient and powerful ultrafast Alexandrite oscillators that will be very attractive for various applications including nonlinear frequency conversion [9-11] and ultrafast spectroscopy [8]. Next chapter demonstrates results of Kerr-Lens mode locking of Alexandrire laser.

Chapter 6: The Femtosecond Kerr-Lens Mode-Locked Alexandrite Laser

In the previous chapter, 380 fs pulses were achieved from Alexandrite laser. In this chapter, generation of 170 fs pulses from a Kerr-lens mode-locked Alexandrite laser is reported. The achieved pulse duration is less than half of the pulse duration obtained by the passively mode-locked Alexandrite laser using an InP/InGaP QD-SESAM. This result can enable the development of efficient and powerful diode-pumped ultrafast Alexandrite oscillators and amplifiers for industrial, scientific and medical applications.

6.1 Kerr-Lens Mode Locking

Ker-lens mode locking (KLM) is an excellent method for generating ultra-short pulses from solid-state lasers that has high modulation depth and fast recovery. The third-order nonlinearity of the gain medium is key to obtaining Kerr-lens mode locking. In this method, the crystal (gain medium) acts as its own saturable absorber so it provides more compact laser cavity. If a pulse with Gaussian intensity profile I(r,z) oscillates in the cavity, where r is the distance from the center of the beam and z is the light propagation direction, the powerful pulse can modulate the refractive index of the gain medium through the nonlinear refractive index n_2 as illustrated in equation (6.1) [92-94]:

$$n(r,z) = n_0 + n_2 I(r,z), \tag{6.1}$$

where n_o is the linear refractive index and n_2 is the nonlinear index of refraction.

Two effects are obtained in gain medium due to Kerr nonlinearity. First, the phase of the pulse modulates itself (self-phase modulation effect), which causes the phase to chirp and to broaden its spectrum. Second, when the high intensity beam passes through the crystal, it provides a virtual lens which focusses the beam. In fact, the refractive index of the medium is related to the intensity strength, so the gain medium acts as a positive lens (if n_2 is positive) due to the modulated refractive index. In this way, non-uniform power density distribution in the Gaussian beam of laser resonators causes refractive index variations through the beam profile. Because the intensity of the Gaussian beam is greater in the center of the beam, according to equation (6.1) the refractive index is higher in the center of the beam than at the edge. Since the temporal and spatial intensity of the pulses is higher in the center than at the edges of the pulse, a positive lens forms. This produces a stronger focus in the central part of the gain medium. Therefore, the medium acts as a positive lens for intense light and this is called self-focusing.

There are two Kerr-lens mode locking methods: hard-aperture and soft-aperture. In the hard-aperture technique, which is used in this study, the loss of unfocused laser beam and pulses can be modulated by using a small diameter aperture located behind the gain medium. In this way, only the very central part of the pulse has high enough intensity to focus the beam to a smaller size and is able to pass the aperture without loss. The leading and trailing edges of the pulse, which have weaker intensity, are removed by the aperture, which causes the production of shorter pulses. This method is called hard-aperture Kerr-lens mode locking because it has a real aperture in the cavity. This is illustrated in Figure 6.1 [72]. However, in soft-aperture Kerr-lens mode locking technique, there is no real aperture in the cavity. In this method, an artificial aperture is provided when the pump beam is intensely focused into the gain medium and forms a small gain volume which is shown in Figure 6.2 [95]. In this way, Kerr lensing focuses the cavity mode into the gain

medium where it overlaps well with the pump mode. Therefore, ultrashort pulses are obtained because, according to the Kerr effect, only the very central part of the lasing pulse, which has high enough intensity, is focused enough to overlap well with the pump mode and become amplified. On the other hand, CW and low intensity light does not overlap with the pump mode sufficiently enough to be amplified [1].

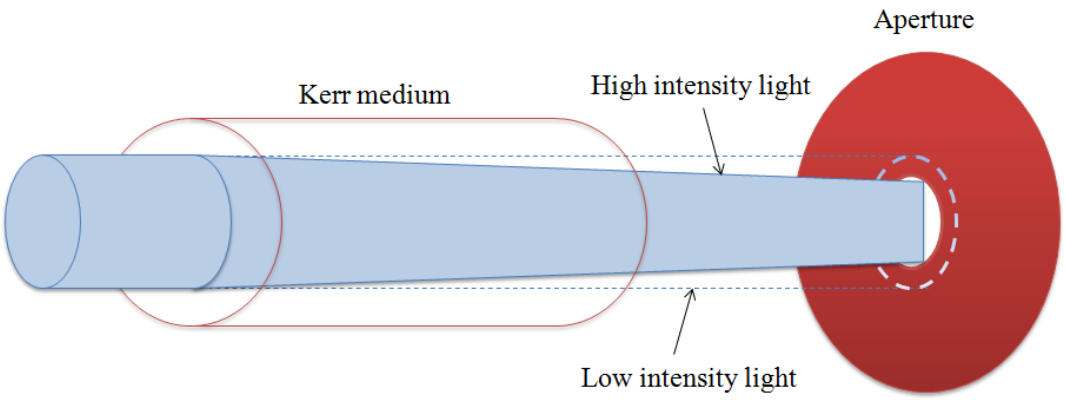

Figure 6.1: Schematic of the hard-aperture Kerr-lens mode locking.

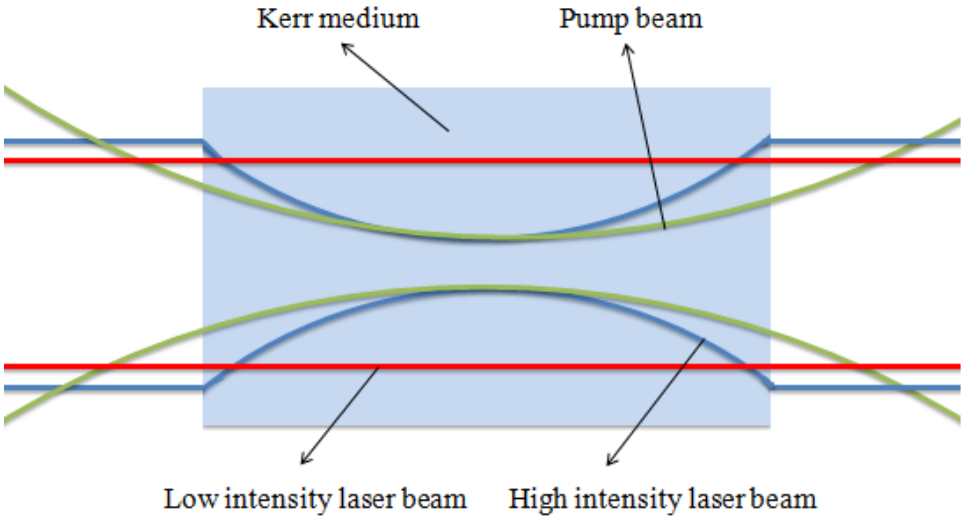

Figure 6.2: Schematic of the soft-aperture Kerr-lens mode locking.

It should be noted that compensation of positive dispersion in resonator is mandatory in order to produce ultrashort pulses.

KLM method is based on the self-focusing effect of light in a resonator using nonlinear properties of gain medium. Both methods (hard-aperture and soft-aperture KLM) need precise alignment of the resonator to provide stable mode locking. In fact, the most important design features of the KLM resonator are its optical stability and focusing conditions in the Kerr medium [82]. The main focus of this section is on hard-aperture KLM when the laser crystal is both a Kerr medium and a gain medium.

The total loss of KLM laser cavities is described by equation (6.2) where L_0 is the total linear loss, k is the nonlinear loss coefficient, and P is the intracavity instantaneous power [96].

$$L = L_0 - kP \,. \tag{6.2}$$

To obtain self-starting mode locking, the coefficient must be large enough to provide an appropriate amount of loss modulation. In fact, a low nonlinear loss coefficient produces low nonlinear loss modulation in the KLM regime, so mode locking cannot self-start. Thus, to maximize loss modulation, the ABCD matrix of the cavity is usually analyzed to find optimal cavity parameters [96].

A common cavity for mode locking is shown in Figure 6.3. In this cavity, the slit is placed in front of M1 to obtain a hard-aperture KLM.

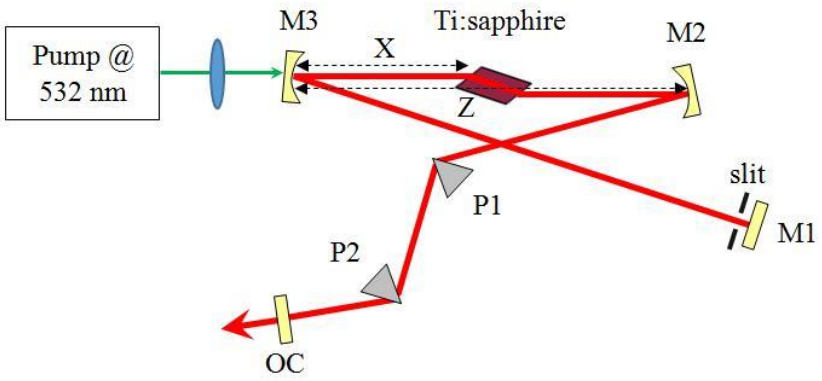

Figure 6.3. Ti:sapphire KLM cavity.

As previously explained, cavity loss is described by equation (6.3), which includes coefficient k (non-linear loss) determined by partial transmission through the slit shown in the Figure 6.3. In equation (6.3), 2a is the width of the slit, P_c is the critical power for self-focusing, and w_1 is the Gaussian beam spot size in the direction that the slit cuts the beam, and it can be calculated by the ABCD matrix. Also, δ in this equation is the beam spot size variation in the slit defined by equation (6.4). In this equation, p is described by equation (6.5), which expresses P as the total cavity power [96].

$$k = -2\sqrt{\frac{2}{\pi}}\exp\left[-2(a/w_1)^2\right]\frac{a}{w_1 P_c}\delta \tag{6.3}$$

$$\delta = \left(\frac{1}{w_1}\frac{dw_1}{dp}\right)_{p=0} \tag{6.4}$$

$$p = P/P_c \tag{6.5}$$

The most important features in designing the KLM cavity is the cavity mode spot size variation on the aperture. This parameter is described in equation (6.4). In fact, if δ has a large negative value, when the high power beam is focused by the Kerr lens, the beam size is reduced

and it passes through the slit without loss as shown in figure 6.1. The maximum δ is obtained at the plane of one of the end mirrors as illustrated in figure 6.3. δ can be calculated by the ABCD matrix model [97-99].

Equation (6.4) was used to design the optimized Kerr lens resonator with the highest beam size variation parameter δ when it is negative. For achieving a large negative value of δ, the cavity should be designed near the stability edge. In fact, to design a resonator suitable for femtosecond self-starting Kerr-lens mode-locked laser, a large negative value of δ should be achieved according to the distance between the focusing mirrors *z* and the distance between a focusing mirror and Kerr medium shown in Figure 6.3 [82].

6.2 Kerr-Lens Mode Locking of Alexandrite Laser

KLM is considered a promising way for mode locking of Alexandrite laser to produce ultrashort pulses [92-94]. The generation of 170 fs pulses from a Ker-lens mode-locked Alexandrite laser was demonstrated for the first time in this study.

6.2.1 Experimental Setup of Kerr-Lens Mode Locking

Kerr-lens mode locking is a powerful and well-known method for generation of ultrashort pulses from solid-state lasers [81] and was investigated as mode locking mechanism in this work. Experimental setup of the Kerr-lens mode-locked Alexandrite oscillator is schematically depicted in Figure 6.4(a). The laser used a slightly modified standard delta cavity which consisted of five mirrors and a Brewster-cut crystal. The designed cavity provided a good overlap between the pump and cavity modes and was similar to the one previously used in the continuous-wave experiments in Chapter 3. Mirrors M1-M4 were typical Ti:sapphire laser mirrors and were highly reflecting

(HR) in the 650-900 nm range. The radii of curvature of the two concave folding mirrors M3 and M4 were 100 mm. Additional mirror M2 with a radius of curvature of 200 mm was used for fine control of the cavity mode size in the crystal. This arm of the cavity also contained a vertical slit to enable a hard-aperture Kerr-lens mode locking. The output coupler (OC) had a 3% transmission around 750 nm.

A 7 mm-long Alexandrite crystal doped with 0.155% of Cr (NG Synoptics) was used in the experiments. The crystal was held in an aluminum crystal holder which was not actively cooled (see Figure 6.4(b)). It was mounted on a translation stage which helped to optimize its position with respect to the pump and cavity mode foci. The crystal was pumped by a CW green laser radiation at 532 nm with up to 8 W (Finesse, Laser Quantum). The pump was focused into a ~45 μm spot size diameter inside the crystal by a 150 mm focal length lens. About 85% of the pump power was absorbed in the crystal.

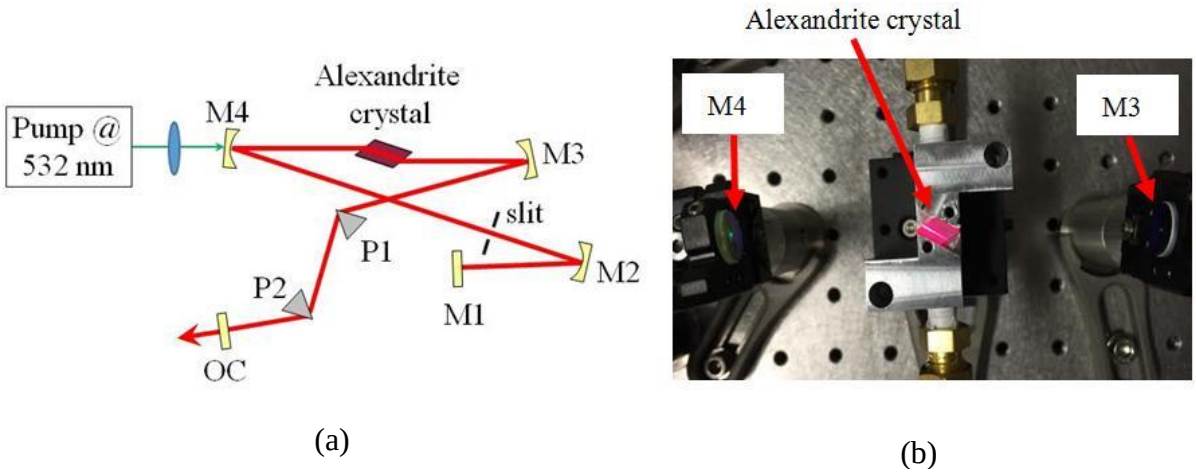

(a) (b)

Figure 6.4. (a) Schematic layout of the femtosecond KLM Alexandrite laser oscillator and a photograph of the laser crystal between the folding mirrors at low pump power. (b) The path of the pump light in the crystal near its center is clearly visualized by the excited fluorescence.

For the design of Alexandrite KLM cavity in this experiment, the traditional formalism outlined in [82] was used. The values of δ from the equation (6.4) can be obtained by solving the simple ABCD law for the KLM cavity [97] and plotted as the Magni plots shown in Figure 6.5. The Magni plots shown in the Figure 6.5 demonstrate different values for δ (explained by equation (6.4)) based on the separation of folding mirrors and the distance between the crystal and the curved mirror of the cavity. Note that negative values of δ indicate areas of enhanced Kerr lensing. The operating point is shown by the red dot in the low misalignment sensitivity region, near its inner stability edge.

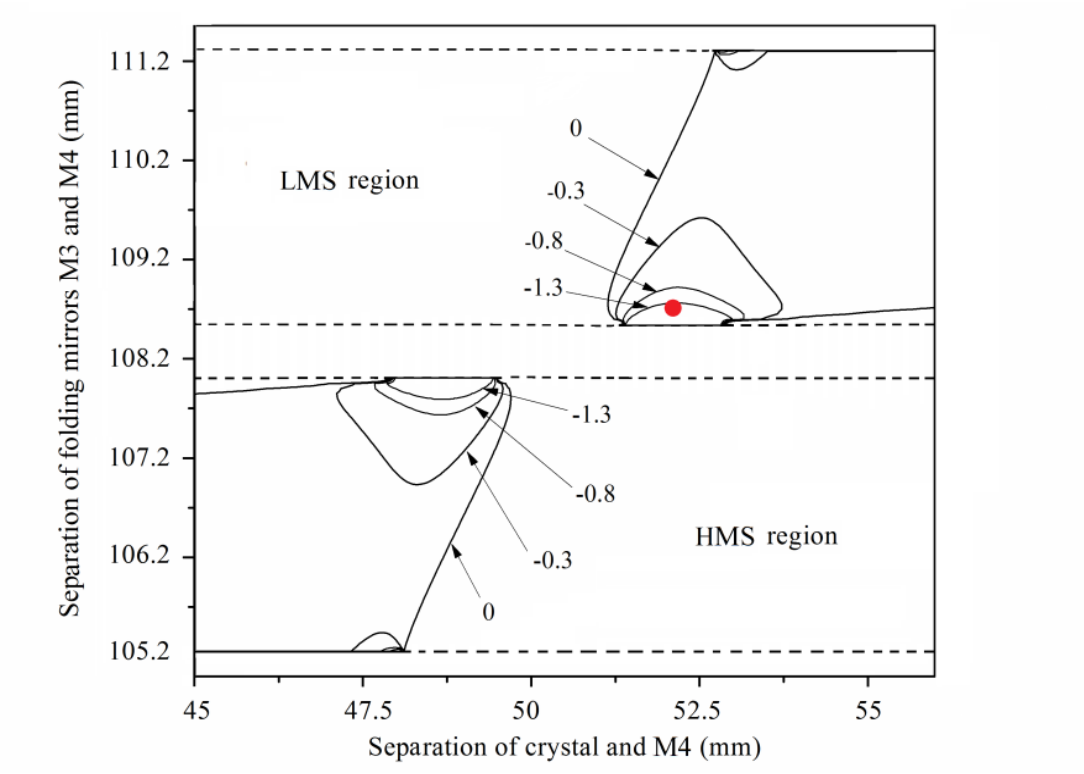

Figure 6.5. Calculated contour Magni plots for the tangential plane of the used KLM resonator. Red dot indicates the operating point. The vertical axis is the separation of folding mirrors M3 and M4, and the horizontal axis indicates the separation of crystal and folding mirror M4. A high misalignment sensitivity region (HMS) and a low misalignment sensitivity region (LMS) are shown.

6.2.2 Results and Discussion

In the initial CW experiments the laser could produce more than 1 W of output power at full pump power. By configuring the laser to operate close to one of the stability edges (as shown in Figure 6.5) and adjusting the width of the vertical slit, a hard-aperture KLM was achieved. This

required careful positioning of the mirror M3 as well as of the crystal. Mode locking was initiated in a usual way, i.e. by small mechanical perturbation such as tapping on a mirror mount.

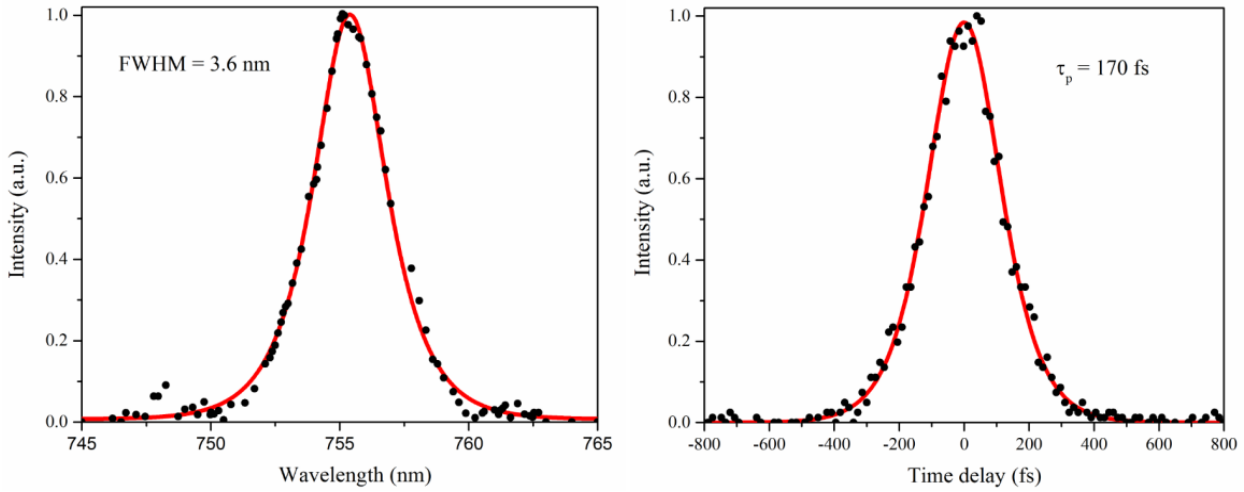

(b) (b)

Figure 6.6. (a) Measured spectrum and (b) autocorrelation trace of the pulses with fits assuming a sech^2 profile.

A maximum average output power of 780 mW was achieved in the mode-locked regime. This corresponds to 9.8% of optical-to-optical efficiency which is comparable to the typical performance of femtosecond Ti:sapphire oscillators [82]. The spectrum was centered at 755 nm and had a FWHM (full width at half maximum) bandwidth of 3.6 nm. The autocorrelation trace of the generated pulses together with the corresponding spectrum are shown in Figure 6.6. The time-bandwidth product of the generated pulses was calculated to be 0.32, indicating that they were close to transform limited.

Single pulse mode locking was ensured by using a long scan range (200 ps) autocorrelator and a high speed oscilloscope with photodiode that had combined resolution of ~100 ps. Therefore,

femtosecond-to-nanosecond time scales were completely covered [3, 76, 78]. An additional RF spectrum measurement indicated that the noise level was suppressed by more than 45 dB with respect to the fundamental mode.

Due to the proximity of the generated wavelengths (~755 nm) to the visible range and intensity of the laser radiation, the beam was clearly visible on a white background. A photograph of the laser beam and its transverse intensity profiles in the CW and mode-locked regimes are shown in Figure 6.7. The laser operated in the fundamental transverse mode with an estimated beam quality factor of $M^2<1.2$.

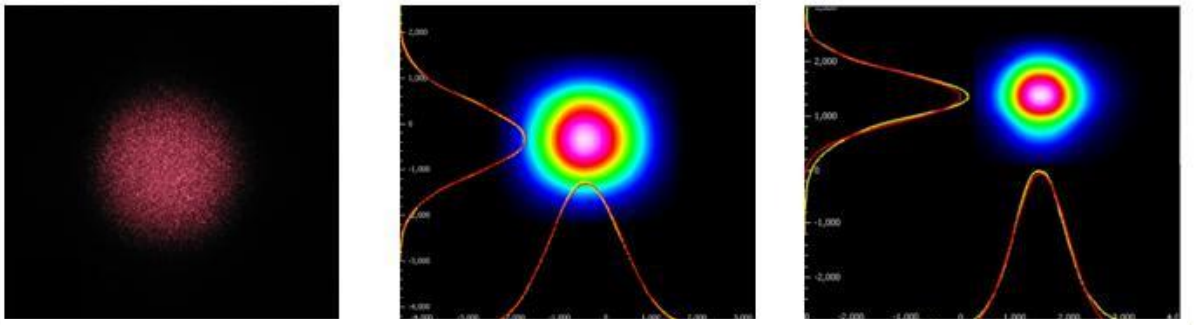

(c) (b) (c)

Figure 6.7. Laser beam on paper surface (a) and its intensity profiles in the CW (b) and mode-locked (c) regimes.

Considering the repetition rate of 80 MHz, the generated laser pulses had energy of ~9.8 nJ and >57 kW of peak power. These are the first femtosecond pulses that were generated from a Kerr-lens mode-locked Alexandrite laser. A photograph of the developed laser is shown in Figure 6.8.

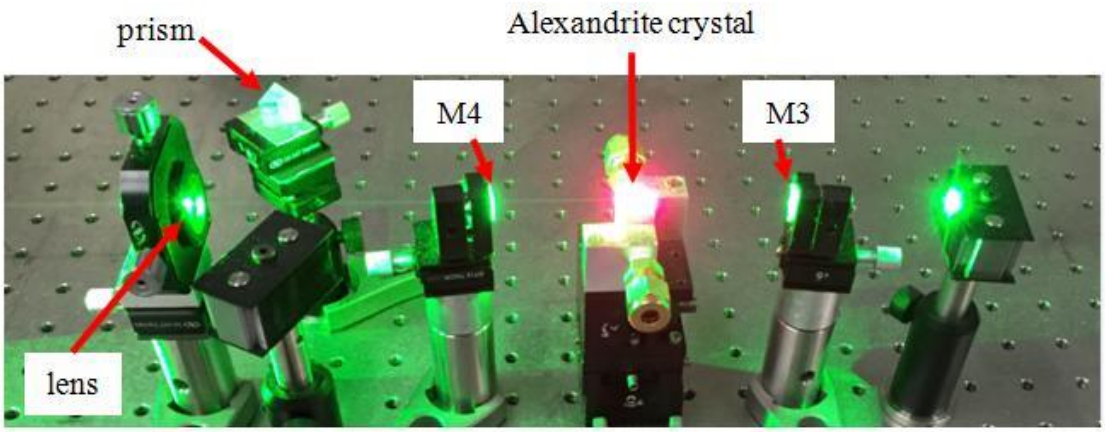

Figure 6.8. Photograph of the pumped Alexandrite crystal in the laser cavity.

6.3 Conclusions

A femtosecond Kerr-lens mode-locked Alexandrite laser was demonstrated. Pulses as short as 170 fs were generated with 780 mW of average output power. Owing to the broad tuning range (~85 nm) of Alexandrite [28] and recent data on its dispersive properties [52] even shorter pulses (down to 10 fs) should be possible with careful dispersion management. The extension to the visible diode pumping opens the way for the development of efficient ultrafast Alexandrite oscillators and amplifiers. With currently available red diode pump powers (>60W) [28], femtosecond operation with an output power in the range of 10 W should be possible. Power scaling can be also explored using thin-disk technology due to the reasonably low quantum defect.

Chapter 7: Conclusions and Future work

7.1 Conclusions

The main focus of this research was to develop an ultrafast Alexandrite laser source that can be considered as a replacement to the broadly used, but inefficient and expensive Ti:sapphire. This laser source is essential for many applications such as spectroscopy, nonlinear biomedical imaging and the study of materials' nonlinear properties. The generation of ultrashort laser pulses was facilitated due to broad emission bandwidth of this crystal. The demonstrated laser systems indicate the ability of Alexandrite lasers to produce ultra-short pulses nearly compatible with those from a Ti:sapphire laser.

For the development of a pulsed oscillator, a high power continuous-wave Alexandrite laser with green pump was built in such a way that it was suitable to be adapted for the mode locking.

The thermal lensing and thermal properties of the continuous-wave Alexandrite laser were evaluated. The results showed a positive thermal lensing effect that needed to be taken into account for the design of the Alexandrite laser oscillators.

Also, due to the growing interest in dual-wavelength operation for the use as an optical source of terahertz (THz) radiation, during the development of the laser system a high power dual-wavelength continuous-wave Alexandrite laser was demonstrated for the first time. In this experiment, different wavelength pairs were generated by using BRFs with different thicknesses.

In addition, femtosecond laser systems were demonstrated by using two different well-known methods: semiconductor saturable absorber and Kerr-lens mode locking. In the first method, an InP/InGaP QD-SESAM was used for mode locking. This saturable absorber mirror was

previously used to produce picoseconds pulses at 800 nm from a Ti:sapphire laser. In this work, femtosecond Alexandrite laser using an InP/InGaP QD-SESAM was developed. Stable passive mode locking at ~775 nm with femtosecond laser pulses (380 and 420 fs) and an average output power of 295 and 325 mW was obtained. Additionally, the generation of the shorter pulses from Alexandrite laser (170 fs) with output power of 780 mW was demonstrated using the Kerr-lens mode locking technique.

This work demonstrated the development of an Alexandrite laser. In fact, the first dual-wavelength and femtosecond operation of Alexandrite lasers were obtained.

7.2 Future Work

Some features of the demonstrated laser systems can be enhanced. In this section, some possible solutions are proposed for improvement of the performance of the demonstrated lasers in terms of efficiency, pulse duration, output power, and applications.

In the future, the use of a red diode pump instead of the green pump can lead to the development of efficient ultrafast Alexandrite oscillators and amplifiers owing to a low quantum defect. In addition, due to the broad emission range (~85 nm) and dispersive properties of Alexandrite lasers, SESAM or Kerr lens mode locking with an optimum dispersion management should lead to the generation of shorter pulses (down to ~10 fs). Also, more efficient mode locking should be possible by creating SESAMs optimized for the laser wavelength of 755 nm where Alexandrite laser has the maximum output power. At the same time the hybrid action of SESAM and Kerr lens mode locking techniques can lead to the generation of reliable sub-100 fs laser pulses. Furthermore, for the case of the CW dual-wavelength laser, different wavelength pairs can be obtained by using different BRF thicknesses. Additionally, passively mode-locked dual-

wavelength Alexandrite laser could be achieved by using a BRF in the mode-locked laser oscillator. Finally, due to its broad band emission spectra in the near-infra red region, this laser can be used as an efficient ultrafast laser source for biomedical applications such as microscopy, spectroscopy, optical coherence tomography and laser surgery.

Appendix A: Beam Quality Measurements

According to measurements, the green laser pump had a fundamental Gaussian mode. By measuring the beam quality (i.e. M^2 parameter) of the Alexandrite laser it was possible to evaluate the effects of thermal lensing described in section 3.4. In this experiment, an infrared spot size was measured for OC=5% from the maximum output power of 1.11 W to 0.09 W for the pump powers from 1.5 W to 6 W with a step of 0.5. The measured spatial profiles of the laser mode from the Alexandrite laser corresponding to various levels of output power from the laser are illustrated in Figure A.1. The data from the spatial profiles were processed by OriginPro Software, and the determined M^2 values were shown in Figure 3.11 for the incident pump power of 6 W. In addition, the determined M^2 values for the other incident pump power are demonstrated in Figure A.2. The Gaussian beam propagation equation, which was used for fitting, in OriginPro Software is shown in equation (A.1) [1] explained in equation (3.2). This formula uses the x and y directions (i.e. horizontal and vertical, respectively) separately.

$$w = w_0 \sqrt{1 + \left(\frac{755 \times 10^{-9} \times M^2 (z - z_0)}{\pi {w_0}^2} \right)^2} \qquad \text{(A.1)}$$

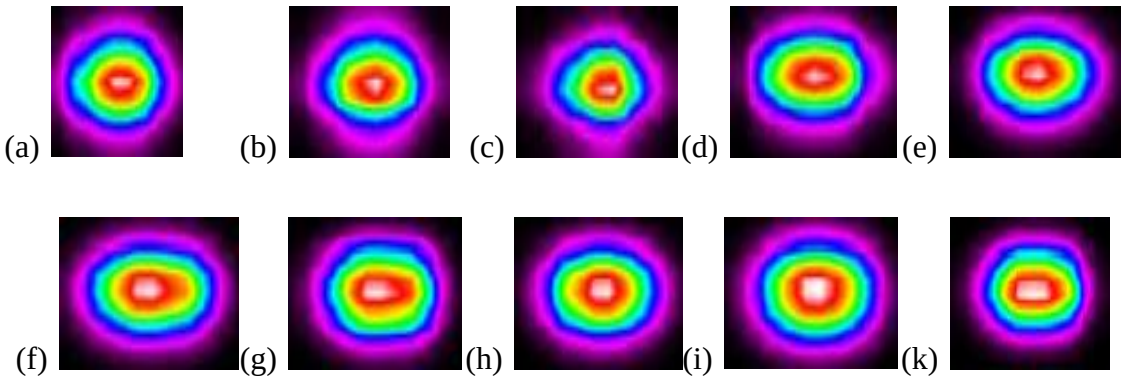

Figure A.1. Spatial profiles of the laser mode from the Alexandrite laser corresponding to the various output power levels: (a) 0.09 W; (b) 0.18 W; (c) 0.27 W; (d) 0.40 W; (e) 0.52 W; (f) 0.65 W; (g) 0.77 W; (h) 0.87 W; (i) 1.0 W; (k) 1.11 W.

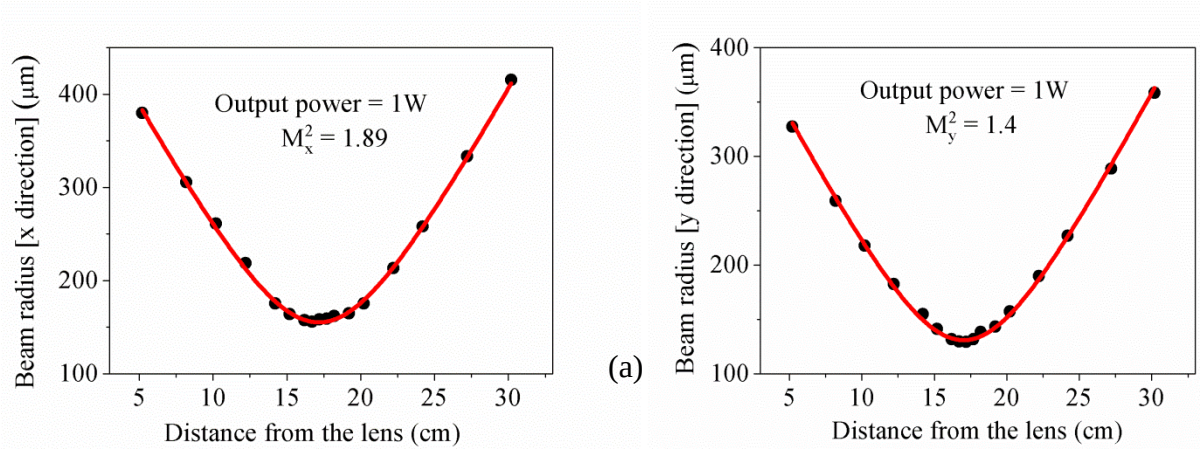

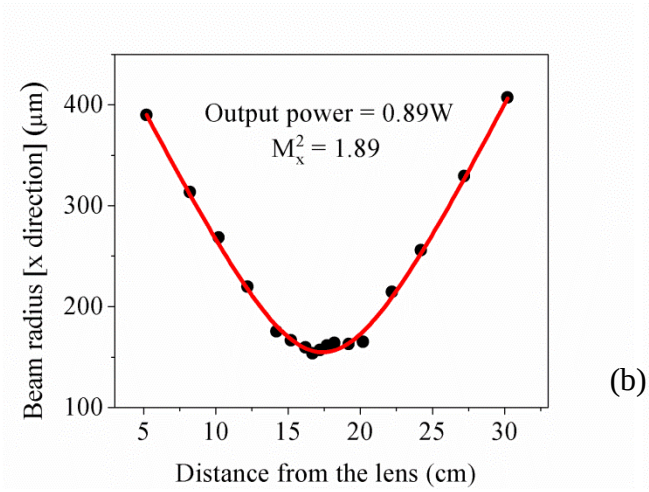
Output power = 0.89W
M_x^2 = 1.89
Beam radius [x direction] (μm)
Distance from the lens (cm)

(b)

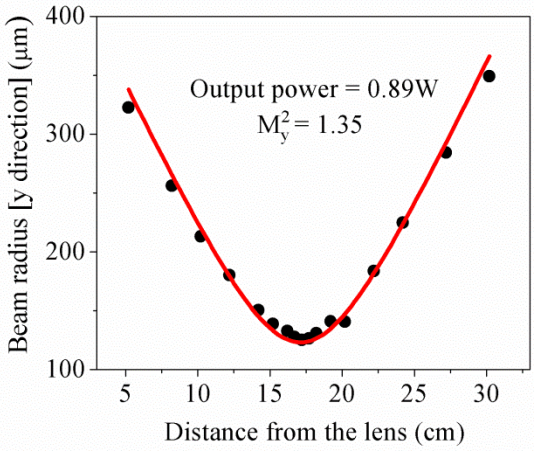
Output power = 0.89W
M_y^2 = 1.35
Beam radius [y direction] (μm)
Distance from the lens (cm)

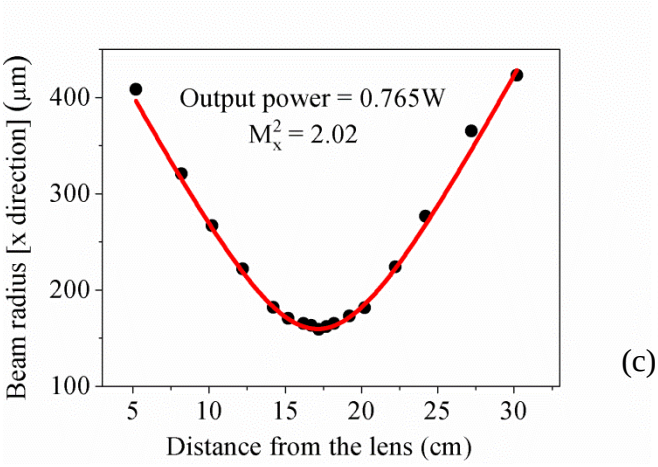
Output power = 0.765W
M_x^2 = 2.02
Beam radius [x direction] (μm)
Distance from the lens (cm)

(c)

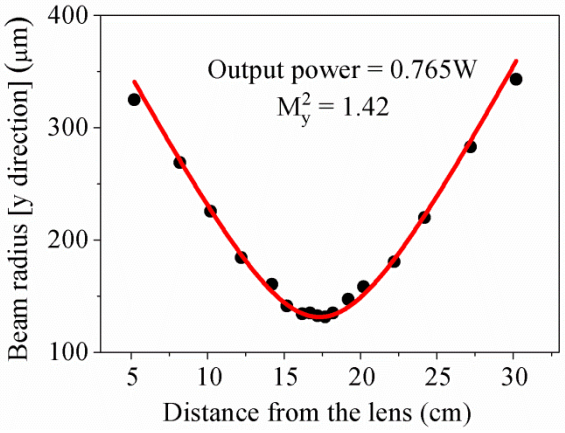
Output power = 0.765W
M_y^2 = 1.42
Beam radius [y direction] (μm)
Distance from the lens (cm)

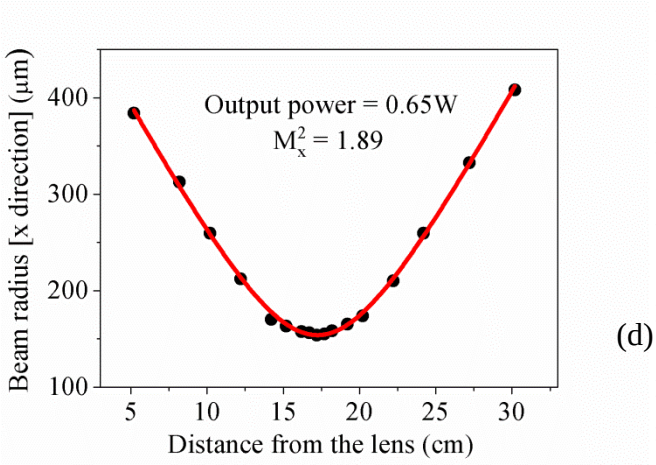
Output power = 0.65W
M_x^2 = 1.89
Beam radius [x direction] (μm)
Distance from the lens (cm)

(d)

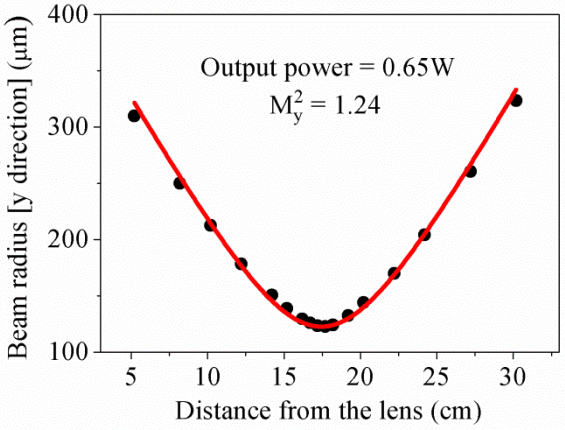
Output power = 0.65W
M_y^2 = 1.24
Beam radius [y direction] (μm)
Distance from the lens (cm)

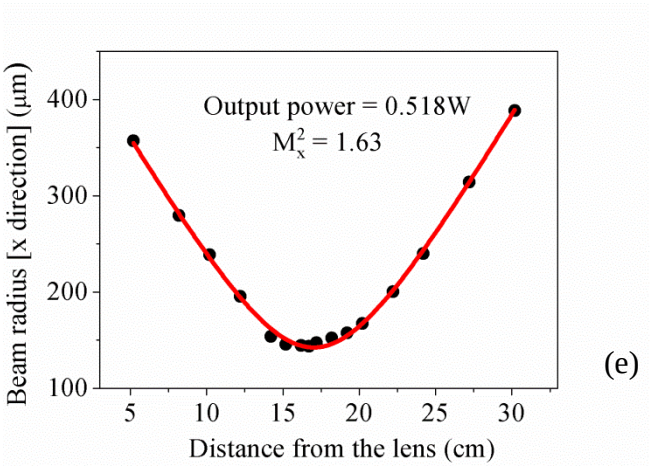
Output power = 0.518W
M_x^2 = 1.63
Beam radius [x direction] (μm)
Distance from the lens (cm)

(e)

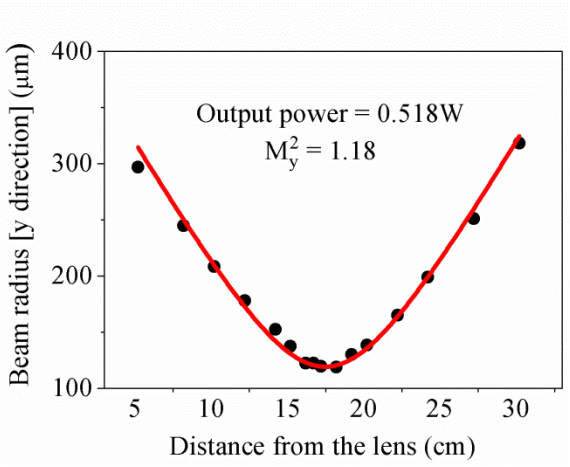
Output power = 0.518W
M_y^2 = 1.18
Beam radius [y direction] (μm)
Distance from the lens (cm)

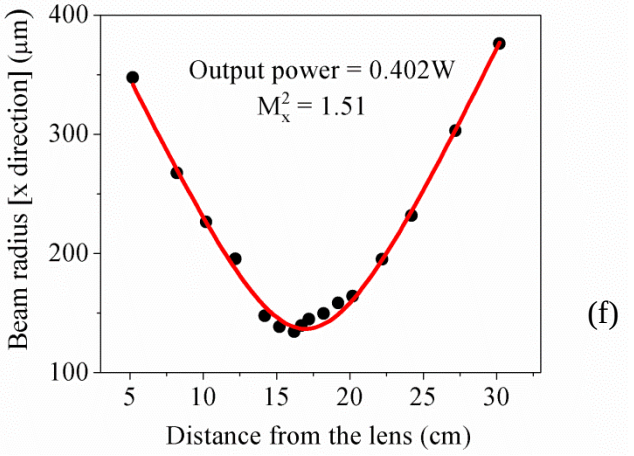
Output power = 0.402W
M_x^2 = 1.51
Beam radius [x direction] (μm)
Distance from the lens (cm)

(f)

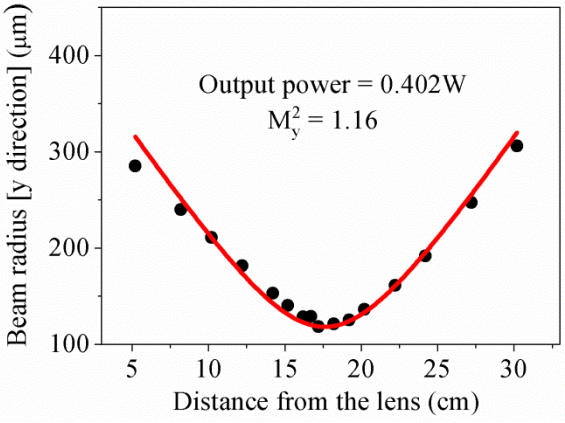
Output power = 0.402W
M_y^2 = 1.16
Beam radius [y direction] (μm)
Distance from the lens (cm)

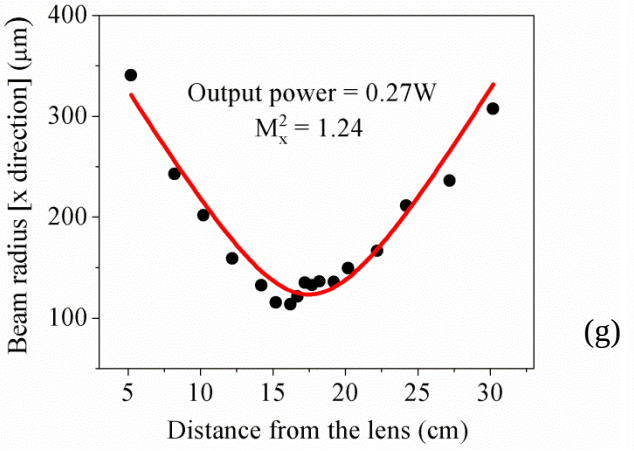
Output power = 0.27W
M_x^2 = 1.24
Beam radius [x direction] (μm)
Distance from the lens (cm)

(g)

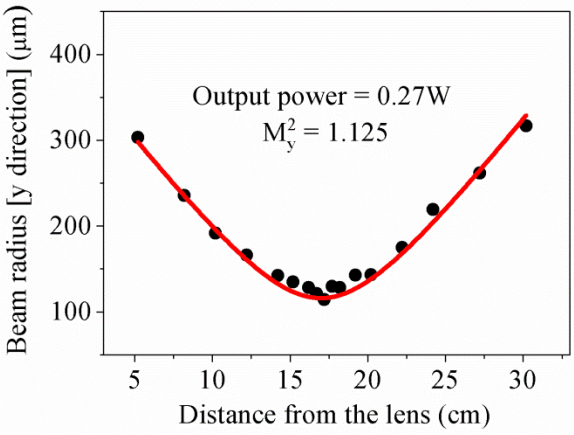
Output power = 0.27W
M_y^2 = 1.125
Beam radius [y direction] (μm)
Distance from the lens (cm)

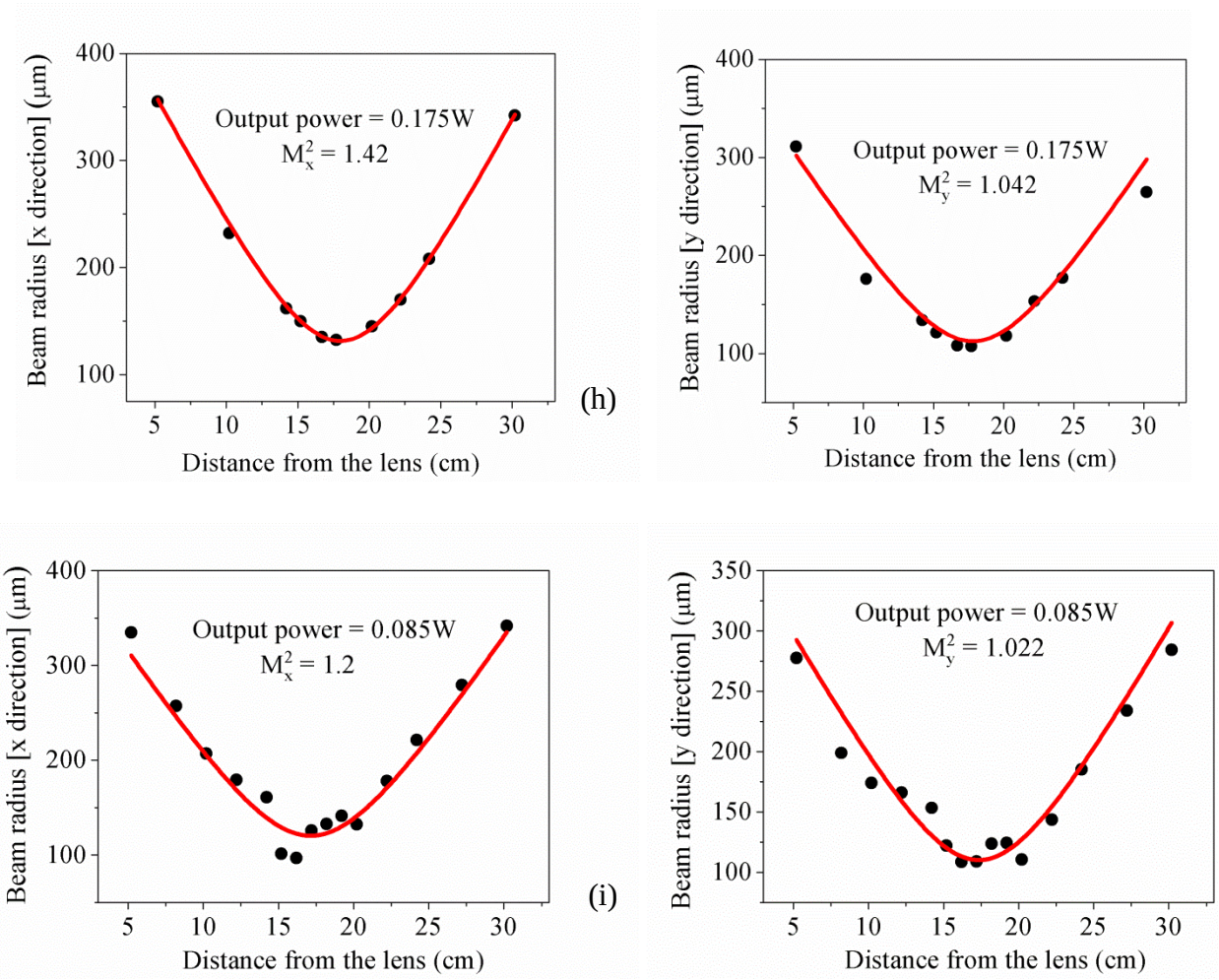

Figure A.2. Evaluation of the beam quality factor M^2 in horizontal direction x and vertical direction y for the Alexandrite laser for the incident pump power other than 6W (a) Pin = 5.5 W; (b) Pin = 5 W; (c) Pin = 4.5 W; (d) Pin = 4 W; (e) Pin = 3.5 W; (f) Pin = 3 W; (g) Pin = 2.5 W; (h) Pin = 2 W; (i) Pin = 1.5 W.

References

[1] W. Koechner and M. Bass, *Solid-State Lasers: A Graduate Text.* New York, NY: Springer, 2003.

[2] K. Lamb, D. E. Spence, J. Hong, C. Yelland, and W. Sibbett, "All-solid-state self-mode-locked Ti:sapphire laser," *Optics Letters*, vol.19, no. 22, pp.1864–1866, 1994.

[3] H. Zhao, and A. Major, "Powerful 67 fs Kerr-lens mode-locked prismless Yb:KGW oscillator," *Optics Express*, vol. 21, no. 26, pp. 31846-31851, 2013.

[4] R. Akbari, K. A. Fedorova, E. U. Rafailov, A. Major, "Diode-pumped ultrafast Yb:KGW laser with 56 fs pulses and multi-100 kW peak power based on SESAM and Kerr-lens mode locking," *Applied Physics B*, vol. 123, no. 4, pp. 123, 2017.

[5] S. Manjooran and A. Major, "Generation of Sub-50 fs Pulses With >1.5 MW of Peak Power From a Diode-Pumped Yb:CALGO Laser Oscillator," in Conference on Lasers and Electro-Optics, OSA Technical Digest, 2016, (Optical Society of America, 2016), paper JTu5A.82.

[6] S. Fischbach, A. Gorbach, D. Di Nuzzo and E. Da Como, "Near infrared ultrafast pump-probe spectroscopy with ZrF4-BaF2-LaF3-AlF3-NaF fiber supercontinuum," *Applied Physics Letters*, vol. 107, no. 2, p. 021103, 2015.

[7] M. H. Vos, F. Rappaport, J.C. Lambry, J. Breton, J.L. Martin, "Visualization of coherent nuclear motion in a membrane protein by femtosecond spectroscopy," *Nature*, vol. 363, no. 6427, p. 320, 1993.

[8] A. Major, J.S. Aitchison, P.W.E. Smith, F. Druon, P. Georges, B. Viana, G.P. Aka "Z-scan measurements of the nonlinear refractive indices of novel Yb-doped laser crystal hosts," *Applied Physics B*, vol. 80, no. 2, pp. 199-201, 2005.

[9] A. Major, D. Sandkuijl, and V. Barzda, "Efficient frequency doubling of a femtosecond Yb:KGW laser in a BiB3O6 crystal," *Optics Express*, vol. 17, no.14 , pp. 12039–12042, 2009.

[10] H. Zhao, I. T. Lima Jr., and A. Major, "Near-infrared properties of periodically poled KTiOPO4 and stoichiometric MgO-doped LiTaO3 crystals for high power optical parametric oscillation with femtosecond pulses," *Laser Physics*, vol. 20, no.6, pp. 1404-1409, 2010.

[11] S. Manjooran, H. Zhao, I. T. Lima Jr., and A. Major, "Phase-matching properties of PPKTP, MgO:PPSLT and MgO:PPcLN for ultrafast optical parametric oscillation in the visible and near-infrared ranges with green pump," *Laser Physics*, vol. 22, n. 8, pp. 1325-1330, 2012.

[12] A. Major, R. Cisek and V. Barzda, "Development of diode-pumped high average power continuous-wave and ultrashort pulse Yb:KGW lasers for nonlinear microscopy," Proc. SPIE vol. 6108, 2006, p. 61080Y.

[13] D. Sandkuijl, R. Cisek, A. Major, and V. Barzda, "Differential microscopy for fluorescence-detected nonlinear absorption linear anisotropy based on a staggered two-beam femtosecond Yb:KGW oscillator," *Biomedical Optics Express*, vol. 1, no. 3, pp. 895-901, 2010.

[14] B. Pearson and T. Weinacht, "Three-in-one microscopy," *Nature Photonics*, vol. 6, no. 2, pp. 78-80, 2012.

[15] P. Antal and R. Szipőcs, "Tunable, low-repetition-rate, cost-efficient femtosecond Ti:sapphire laser for nonlinear microscopy," *Applied Physics B*, vol. 107, no. 1, pp. 17-22, 2011.

[16] P. Prasad, *Introduction to Biophotonics*. Hoboken: Wiley, 2004.

[17] J. G. Fujimoto, A. D. Aguirre, Y. Chen, P. R. Herz, P.-L. Hsiung, T. H. Ko, N. Nishizawa, and F. X. Kärtner, "Ultrahigh-Resolution Optical Coherence Tomography Using Femtosecond Lasers," in *Ultrashort Laser Pulses in Biology and Medicine*, M. Braun, P. Gilch, and W. Zinth, Eds. Berlin, Heidelberg: Springer, 2008, pp. 3–27.

[18] J. G. Fujimoto, "Optical coherence tomography for ultrahigh resolution in vivo imaging," *Nature Biotechnology*, vol. 21, no. 11, pp. 1361–1367, 2003.

[19] S. Park, K. Kwak, and M. D. Fayer, "Ultrafast 2D-IR vibrational echo spectroscopy: a probeof molecular dynamics," *Laser Physics Letters*, vol. 4, no. 10, pp. 704-718, 2007.

[20] Q. Fu, G. Mak, and H. M. Van Driel, "High-power, 62-fs infrared optical parametric oscillator synchronously pumped by a 76-MHz Ti:sapphire laser," *Optics Letters*, vol. 17, no 14, pp. 1006-1008, 1992.

[21] A. F. Pegoraro, A. Ridsdale, D. J. Moffatt, Y. Jia, J. P. Pezacki, and A. Stolow, "Optimally chirped multimodal CARS microscopy based on a single Ti:sapphire oscillator," *Optics Express*, vol. 17, no. 4, pp. 2984-2996, 2009.

[22] H. K. Soong, and J. B. Malta, "Femtosecond lasers in ophthalmology," *American journal of ophthalmology*, Vol. 147, no. 2, pp. 189-197, 2009.

[23] A. Vogel, J. Noack, G. Hüttman, and G. Paltauf, "Mechanisms of femtosecond laser nanosurgery of cells and tissues," *Applied Physics B*, vol. 81, no. 8, pp. 1015-1047, 2005.

[24] R. Ell, U. Morgner, F. X. Kartner, J. G. Fujimoto, E. P. Ippen, V. Scheuer, G. Angelow, T. Tschudi, M. J.Lederer, A. Boiko, and B. Luther-Davies, "Generation of 5-fs pulses and octave-spanning spectra directly from a Ti:sapphire laser," *Optics Letters*, vol. 26, no. 6, pp. 373–375, 2001.

[25] I. D. Jung, F. X. Kärtner, N. Matuschek, D. H. Sutter, F. Morier-Genoud, G. Zhang, U. Keller, V. Scheuer, M. Tilsch, and T. Tschudi, "Self-starting 6.5-fs pulses from a Ti: sapphire laser," *Optics Letters*, vol. 22, no. 13, pp. 1009-1011, 1977.

[26] J. C. Walling, H. P. Jenssen, R. C. Morris, E. W. O'Dell, and O. G. Peterson, "Tunable laser performance in BeAl2O4:Cr3+," *Optics Letters*, vol. 4, no. 6, pp. 182–183, 1979.

[27] J. C. Walling, D. Heller, H. Samelson, D. Harter, J. Pete, and R. Morris, "Tunable Alexandrite lasers: development and performance," *IEEE Journal of Quantum Electronics*, vol. 21, no.10, pp. 1568-1581, 1985.

[28] S. Ghanbari and A. Major, "High power continuous-wave Alexandrite laser with green pump," *Laser Physics*, vol. 26, no. 7, p. 075001, 2016.

[29] A. Teppitaksak, A. Minassian, G. M. Thomas, and M. J. Damzen, "High efficiency >26 W diode end-pumped Alexandrite laser," *Optics Express*, vol. 22, no. 13, pp. 16386–16392, 2014.

[30] R. Scheps, B. M. Gately, J. F. Myers, J. S. Krasinski, and D. F. Heller, "Alexandrite laser pumped by semiconductor lasers," *Applied Physics Letters*, vol. 56, no.23, pp. 2288-2290, 1990.

[31] E. Beyatli, I. Baali, B. Sumpf, G. Erbert, A. Leitenstorfer, A. Sennaroglu and U. Demirbas, "Tapered diode-pumped continuous-wave Alexandrite laser," *Journal of the Optical Society of America B*, vol. 30, no. 12, pp. 3184-3192, 2013.

[32] J. Walling, O. Peterson, H. Jenssen, R. Morris and E. O'Dell, "Tunable Alexandrite lasers," *IEEE Journal of Quantum Electronics*, vol. 16, no. 12, pp. 1302-1315, 1980.

[33] R. Scheps, J. Myers, T. Glesne and H. Serreze, "Monochromatic end-pumped operation of an Alexandrite laser," *Optics communications*, vol. 97, no. 5-6, pp. 363-366, 1993.

[34] H. Samelson, J. Walling, T. Wernikowski and D. Harter, "CW arc-lamp-pumped Alexandrite lasers," *IEEE Journal of Quantum Electronics*, vol. 24, no. 6, pp. 1141-1150, 1988.

[35] V. Lisitsyn, V. Matrosov, V. Orekhova, E. Pestryakov, B. Sevast'yanov, V. Trunov, V. Zenin and Y. Remigaĭlo, "Generation of 0.7–0.8 μ picosecond pulses in an Alexandrite laser with passive mode locking," *Soviet Journal of Quantum Electronics*, vol. 12, no. 3, pp. 368-370, 1982.

[36] R.C. Powell, L. Xi, X. Gang, G. J. Quarles, and J.C. Walling," Spectroscopic properties of alexandrite crystals", *Physical Review B*, vol. *32*, no. 5, pp. 2788, 1985.

[37] "File:Alexandrite structure.png" Wikkimedia Commons [Online], (May, 2014). Available: https://commons.wikimedia.org/wiki/File:Alexandrite_structure.png [April, 14, 2018].

[38] E. Sorokin, I. Sorokina and E. Wintner, "Diode-pumped ultra-short-pulse solid-state lasers," *Applied Physics B*, vol. 72, no. 1, pp. 3-14, 2001.

[39] M. Shand and H. Jenssen, "Temperature dependence of the excited- state absorption of Alexandrite," *IEEE Journal of Quantum Electronics*, vol. 19, no. 3, pp. 480-484, 1983.

[40] E. Sorokin, "Solid-state materials for few-cycle pulse generation and amplification" *in Few-Cycle Laser Pulse Generation and Its Applications*, F. X. Kärtner, Eds. Berlin, Heidelberg: Springer, 2004, pp. 3-73.

[41] S. Guch and C. Jones, "Alexandrite-laser performance at high temperature," Optics Letters, vol. 7, no. 12, p. 608, 1982.

[42] I. Yorulmaz, E. Beyatli, A. Kurt, A. Sennaroglu and U. Demirbas, "Efficient and low-threshold Alexandrite laser pumped by a single-mode diode," *Optical Materials Express*, vol. 4, no.4, pp. 776-789, 2014.

[43] S. Lai and M. Shand, "High efficiency cw laser-pumped tunable Alexandrite laser," *Journal of applied physics*, vol. 54, no. 10, pp. 5642-5644, 1983.

[44] J. Kuper and D. Brown, "High efficiency CW green-pumped Alexandrite," Proc. SPIE, 2006, vol. 6100, p. 61000T.

[45] H. Zhao and A. Major, "Orthogonally polarized continuous wave dual-wavelength Yb:KGW laser induced by thermal lensing," *Applied Physics B*, vol. 122, no. 6, p. 163 (2016).

[46] R. Akbari, H. Zhao and A. Major, "High power continuous wave dual-wavelength operation of a diode-pumped Yb:KGW laser," *Optics Letters*, vol. 41, no. 7, pp. 1601–1604, 2016.

[47] C. W. Luo, Y. Q. Yang, I. T. Mak, Y. H. Chang, K. H. Wu, and T. Kobayashi, "A widely tunable dual-wavelength CW Ti: sapphire laser with collinear output," *Optics Express*, vol. 16, no. 5, pp. 3305-3309, 2008.

[48] M. Hyodo, M. Tani, S. Matsuura, N. Onodera, and K. Sakai, "Generation of millimeter-wave radiation using a dual-longitudinal-mode microchip laser," *Electronic Letters*, vol. 32, no. 17, pp. 1589–1591, 1996.

[49] P. H. Siegel, "Terahertz technology," *IEEE Transactions on microwave theory and techniques*, vol. 50, no. 3, pp. 910–928, 2002.

[50] E. R. Brown, K. A. McIntosh, K. B. Nichols, and C. L. Dennis, "Photomixing up to 3.8 THz in low-temperature-grown GaAs," *Applied Physics Letters*, vol. 66, no. 3, pp. 285–287, 1995.

[51] S. Ghanbari, R. Akbari, and A. Major, "Femtosecond Kerr-lens mode-locked Alexandrite laser," *Optics Express*, vol. 24, no. 13, pp. 14836-14840, 2016.

[52] P. Loiko and A. Major, "Dispersive properties of Alexandrite and beryllium hexaaluminate crystals," *Optical Materials Express*, vol. 6, no. 7, pp. 2177-2183, 2016.

[53] E.A. Arbabzadah and M.J. Damzen, "Fibre-coupled red diode-pumped Alexandrite TEM00 laser with single and double-pass end-pumping," *Laser Physics Letters*, vol. 13, no. 6, p. 065002, 2016.

[54] J. M. Evans, D. E. Spence, D. Burns, and W. Sibbett, "Dual-wavelength self-mode-locked Ti: sapphire laser," *Optics Letters*, vol. 18, no. 3, pp. 1074-1076, 1993.

[55] C. G. Treviño-Palacios, O. J. Zapata-Nava, E. V. Mejía-Uriarte, N. Qureshi, G. Paz-Martínez, and O. Kolokolstev, "Dual wavelength continuous wave laser using a birefringent filter," *Journal of the European Optical Society-Rapid publications*, vol. 8, pp. 1–5, 2013.

[56] M. Katsuragawa, and O. Takashi, "Dual-wavelength injection-locked pulsed laser," *Optics Letters*, vol. 30, no. 18, pp. 2421-2423, 2005.

[57] N. Saito, K. Akagawa, S. Wada, and H. Tashiro, "Dual wavelength oscillation by electronic tuning of a Ti:sapphire laser for difference-frequency generation," in Conference on Lasers and Electro-Optics, D. Scifres and A. Weiner, eds., (The Optical Society of America, 1998), paper CTuC5.

[58] H. Zhao and A. Major, "Dynamic characterization of intracavity losses in broadband quasi-three-level lasers," *Optics Express*, vol. 22, no. 22, pp. 26651-26658, 2014.

[59] A. Major, D. Sandkuijl, and V. Barzda, "A diode-pumped continuous-wave Yb:KGW laser with Ng-axis polarized output," *Laser Physics Letters*, vol. 6, no. 11, pp. 779-781, 2009.

[60] H. Zhao and A. Major "A continuous wave Yb:KGW laser with polarization-independent pump absorption," *Laser Physics*, vol. 23, no. 9, p. 095001, 2013.

[61] D. Xin, M. Hong-Mei, Z. Lei, Z. Yue, W. Wu-Qi, W. Peng, and Y, Jian-Quan, "An all-solid-state high power quasi-continuous-wave tunable dual-wavelength Ti: sapphire laser system using birefringence filter," *Chinese Physics*, vol. 16, no. 7, p. 1991, 2007.

[62] T. Waritanant and A. Major, "Diode-pumped Nd:YVO4 laser with discrete multi-wavelength tunability and high efficiency," *Optics Letters*, vol. 42, no. 6 , pp. 1149–1152, 2017.

[63] G. Holtom, and O. Teschke. "Design of birefringent filter for high-power dye lasers," *IEEE Journal of Quantum Electronics*, vol. 10, no. 8, pp. 577-579, 1974.

[64] K. Naganuma , G. Lenz, and E. P. Ippen, "Variable bandwidth birefringent filter for stable femtosecond lasers," *IEEE Journal of Quantum Electronics*, vol. 28, no. 10, pp. 2142-2150, 1992.

[65] S. Zhu, "Birefringent filter with tilted optic axis for tuning dye lasers: theory and design," *Applied Optics*, vol. 29, no. 3 , pp. 410-415, 1990.

[66] P. Loiko, S. Manjooran, K. Yumashev, and A. Major, "Polarization anisotropy of thermal lens in Yb:KY(WO4)2 laser crystal under high-power diode pumping," *Applied Optics*, vol. 56, no. 10, pp. 2937–294, 2017.

[67] H. Mirzaeian, S. Manjooran, and A. Major, "A simple technique for accurate characterization of thermal lens in solid state lasers," Proc. SPIE, vol. 9288, 2014, p. 928802.

[68] T. Waritanant and A. Major, "Thermal lensing in Nd:YVO4 laser with in-band pumping at 914 nm," *Applied Physics B*, vol. 122, no. 5, p. 135, 2016.

[69] R. Paschotta: Passive Mode Locking. https://www.rp-photonics.com/passive_mode_locking.html. 2008. Copyright Wiley-VCH Verlag GmbH & Co. KGaA.

[70] R. Paschotta: Mode Locking. https://www.rp-photonics.com/mode_locking.html. 2008. Copyright Wiley-VCH Verlag GmbH & Co. KGaA.

[71] "Semiconductor Saturable Absorber Mirrors" in RP Photonics Encyclopedia [Online], (n.d). Available: https://www.rp-photonics.com/semiconductor_saturable_absorber_mirrors.html [January, 25, 2018].

[72] U. Keller, "Recent developments in compact ultrafast lasers," *Nature*, vol. 424, no. 6950, pp. 831-838, 2003.

[73] U. Keller, K. J. Weingarten, F. X. Kartner, D. Kopf, B. Braun, I. D.Jung, R. Fluck, C. Honninger, N.Matuschek, and J. Aus der Au, "Semiconductor saturable absorber mirrors (SESAM's) for femtosecond to nanosecond pulse generation in solid-state lasers," *IEEE Journal of Selected Topics in Quantum Electronics*, vol. 2, no. 3, pp. 435-453, 1996.

[74] C. Hönninger, R. Paschotta, F. Morier-Genoud, M. Moser, and U. Keller, "Q-switching stability limits of continuous-wave passive mode locking," *Journal of the Optical Society of America B*, vol. 16, no. 1, pp. 46-56, 1999.

[75] A. Major, L. Giniunas, N. Langford, A.I. Ferguson, D. Burns, E. Bente, and R. Danielius, "Saturable Bragg reflector-based continuous-wave mode locking of Yb:KGd(WO4)2 laser," *Journal of Modern Optics*, vol. 49, no. 5, pp. 787-793, 2002.

[76] H. Zhao and A. Major, "Megawatt peak power level sub-100 fs Yb:KGW oscillators," *Optics Express*, vol. 22, no. 25, pp. 30425-30431, 2014.

[77] R. Akbari, H. Zhao, K. A. Fedorova, E. U. Rafailov, and A. Major, "Quantum-dot saturable absorber and Kerr-lens mode-locked Yb:KGW laser with >450 kW of peak power," *Optics Letters*, vol. 41, no. 16, pp. 3771–3774, 2016.

[78] T. Waritanant and A. Major, "High efficiency passively mode-locked Nd:YVO4 laser with direct in-band pumping at 914 nm," *Optic Express*, vol. 24, no. 12, pp. 12851–12855, 2016.

[79] A. Major, N. Langford, Th. Graf, D. Burns, and A.I. Ferguson, "Diode-pumped passively mode-locked Nd:KGd(WO4)2 laser with 1W average output power," *Optics Letters*, vol. 27, no. 16 , pp. 1478–1480, 2002.

[80] T. Waritanant and A. Major, "Discretely selectable multiwavelength operation of a semiconductor saturable absorber mirror mode-locked Nd:YVO4 laser," *Optics Letters*, vol. 42, no. 17, pp. 3331-3334, 2017.

[81] D. Spence, P. Kean and W. Sibbett, "60-fsec pulse generation from a self-mode-locked Ti:sapphire laser," *Optics Letters*, vol. 16, no. 1, pp. 42-44, 1991.

[82] G. Cerullo, S. De Silvestri, V. Magni and L. Pallaro, "Resonators for Kerr-lens mode-locked femtosecond Ti:sapphire lasers," *Optics Letters*, vol. 19, no. 11, pp. 807-809, 1994.

[83] S. A. Zolotovskaya, K.G. Wilcox, A. Abdolvand, D.A. Livshits, E.U. Rafailov, "Electronically controlled pulse duration passively mode-locked Cr:Forsterite laser," *IEEE Photonics Technology Letters*, vol. 21, no. 16, pp. 1124-1126, 2009.

[84] F. Völker, Q. Lü, and H. Weber, "Passive mode-locking of an Alexandrite laser for picosecond pulse generation," *Journal of Applied Physics*, vol. 69, no. 6, pp. 3432-3439, 1991.

[85] U. Parali, X. Sheng, A. Minassian, G. Tawy, J. Sathian, G. M. Thomas, and M. J. Damzen, "Diode-pumped Alexandrite laser with passive SESAM Q-switching and wavelength tenability," *Optics Communications*, vol. 410, pp. 970-976, 2017.

[86] V. G. Savitski, P. J. Schlosser, J. E. Hastie, A. B. Krysa, J. S. Roberts, M. D. Dawson, D. Burns, and S. Calvez, "Passive mode-locking of a Ti:Sapphire laser by InGaP quantum-dot saturable absorber," *IEEE Photonics Technology Letters*, vol. 22, no. 4, pp. 209-211, 2010.

[87] M. Butkus, G. Robertson, G. Maker, G. Malcolm, C. Hamilton, A. B. Krysa, B. J. Stevens, R. A. Hogg, Y. Qiu, T. Walther, E. U. Rafailov, "High repetition rate Ti: sapphire laser mode-locked by InP quantum-dot saturable absorber," *IEEE Photonics Technology Letters*, vol. 23, no. 21, pp. 1603-1605, 2011.

[88] A. A. Lagatsky, C. G. Leburn, C. T. A. Brown, W. Sibbett, S. A. Zolotovskaya, and E. U. Rafailov, "Ultrashort-pulse lasers passively mode locked by quantum-dot-based saturable absorbers," *Progress in Quantum Electronics*, vol. 34, no. 1, pp. 1-45, 2010.

[89] E. U. Rafailov, S. J. White, A. A. Lagatsky, A. Miller, W. Sibbett, D. A. Livshits, A. E. Zhukov, and V. M. Ustinov, "Fast Quantum-Dot Saturable Absorber for Passive Mode-Locking of Solid-State Lasers," *IEEE Photonics technology letters*, vol. 16, no. 11, pp. 2439-2441, 2004.

[90] A. A. Lagatsky, F. M. Bain, C. T. A. Brown, W. Sibbett, D. A. Livshits, G. Erbert, and E. U. Rafailov, "Low-loss quantum-dot-based saturable absorber for efficient femtosecond pulse generation," *Applied Physics Letters*, vol. 91, no. 23, p. 231111, 2007.

[91] N. Meiser, K. Seger, V. Pasiskevicius, H. Jang, E. Rafailov, and I. Krestnikov, "Gigahertz repetition rate mode-locked Yb:KYW laser using self-assembled quantum dot saturable absorber," *Applied Physics B*, vol. 110, no. 3, pp. 327-333, 2013.

[92] J. Herrmann, "Theory of Kerr-lens mode locking: role of self-focusing and radially varying gain," *Journal of the Optical Society of America B*, vol. 11, no. 3, p. 498, 1994.

[93] P. Weinberger, "John Kerr and his effects found in 1877 and 1878," *Philosophical Magazine Letters*, vol. 88, no.12, pp. 897-907, 2008.

[94] M. Melnichuk and L. Wood, "Direct Kerr electro-optic effect in noncentrosymmetric materials," *Physical Review A*, vol. 82, no. 1, p. 013821, 2010.

[95] "Kerr-lens modelocking" in Wikipedia [Online], (September, 2017). Available: http://en.wikipedia.org/wiki/Kerr-lens_modelocking [January 25, 2018].

[96] G. Cerullo, S. De Silvestri and V. Magni, "Self-starting Kerr-lens mode locking of a Ti:sapphire laser," *Optics Letters*, vol. 19, no. 14, pp. 1040-1042, 1994.

[97] V. Magni, G. Cerullo and S. De Silvestri, "ABCD matrix analysis of propagation of gaussian beams through Kerr media," *Optics Communications*, vol. 96, no. 4-6, pp. 348-355, 1993.

[98] V. Magni, G. Cerullo and S. De Silvestri," Closed form gaussian beam analysis of resonators containing a Kerr medium for femtosecond lasers," *Optics Communications*, vol. 101, no. 5-6, pp. 365-370, 1993.

[99] J. Xia and M. Lee, "Analysis of cavities for self-starting Kerr-lens mode-locked lasers," *Applied Optics*, vol. 41, no. 3, pp. 453-458, 2002.